European Journal of Radiology 166 (2023) 110984

Contents lists available at ScienceDirect

European Journal of Radiology

journal homepage: www.elsevier.com/locate/ejrad

Review

Extraprostatic incidental findings on prostate mpMRI: A pictorial review from the ESUR junior network

Andrea Ponsiglione [a,1,*], Irene Campo [b,1], Camilla Sachs [c], Carmelo Sofia [d], Eduardo Álvarez-Hornia Pérez [e], Riccardo Ciabattoni [f], Doaa E. Sharaf [g], Pamela Causa-Andrieu [h], Arnaldo Stanzione [a], Renato Cuocolo [i], Jeries Zawaideh [j], Giorgio Brembilla [k]

[a] Department of Advanced Biomedical Sciences, University of Naples Federico II, Naples, Italy
[b] Radiology Unit, Department of Medical, Surgical and Health Sciences, University of Trieste, Trieste, Italy
[c] Department of Radiology, Ospedale Ca' Foncello, 31100, Treviso, Italy
[d] Department of Biomedical Sciences and Morphologic and Functional Imaging, Policlinico Universitario G. Martino, University of Messina, Messina, Italy
[e] Radiology Department, Clinic IMQ Zorrotzaurre, Bilbao, Spain
[f] Department of Radiology, Ospedale San Salvatore di Pesaro, Azienda Sanitaria Territoriale Pesaro Urbino, Pesaro, Italy
[g] Department of Radiology, Urology & Nephrology Center, Mansoura University, Mansoura, Egypt
[h] Department of Radiology, Memorial Sloan Kettering Cancer Center, NY, USA
[i] Department of Medicine, Surgery and Dentistry, University of Salerno, Baronissi, Italy
[j] Department of Radiology, IRCCS Ospedale Policlinico San Martino, Genoa, Italy
[k] Department of Radiology, IRCCS San Raffaele Scientific Institute, Vita-Salute San Raffaele University, Milan, Italy

ARTICLE INFO

Keywords:
mpMRI
Prostate
Extraprostatic
Incidental
Checklist
Review

ABSTRACT

The role of multiparametric MRI (mpMRI) in prostate cancer setting is increasingly consolidated and, as a result, its usage in clinical practice is in exponential growth. However, beyond the prostate gland, several key structures are included in the field of view of mpMRI scans. Consequently, various extra-prostatic incidental findings (IFs) belonging to different anatomical systems can be accidentally recognized. Therefore, it is mandatory for a radiologist to be familiar with the wide range of pathologies potentially encountered, to guide management and avoid patient anxiety and costs due to additional work-up prompted by clinically insignificant extra-prostatic findings. With this pictorial review, we aim to illustrate a wide range of IFs that can be detected when performing mpMRI of the prostate, focusing on their imaging characteristics, differential diagnosis, and clinical relevance. Additionally, we propose the CheckDEEP, the Checklist for DEtection of ExtraProstatic findings, to be used for a thorough evaluation of target areas within each anatomical system.

1. Introduction

In the last decade, there has been an ever-growing interest in magnetic resonance imaging (MRI) of the prostate [1–4]. The updated version of the European Association of Urology guidelines confirmed its role for prostate cancer (PCa) detection while reinforcing its use in the context of active surveillance due to improved detection of clinically significant lesions [5]. The current reference standard for prostate MRI acquisition, interpretation and reporting is represented by the Prostate Imaging-Reporting and Data System (PI-RADS) version 2.1 [6]. According to PI-RADSv2.1 guidelines, the multiparametric MRI (mpMRI) protocol consists of three mandatory sequences: i) T2-weighted (T2w), ii) diffusion weighted (DWI) and iii) dynamic contrast enhanced (DCE) sequences [4,6]. However, in addition to the prostate gland, several key structures are included in the field of view (FOV) of the image. Consequently, extra-prostatic incidental findings (IFs) related to various

Abbreviations: MRI, magnetic resonance imaging; PCa, prostate cancer; PI-RADS, Prostate Imaging-Reporting and Data System; T2w, T2-weighted; DWI, diffusion weighted imaging; DCE, dynamic contrast enhanced; FOV, field of view; IFs, incidental findings; SV, seminal vesicle; mpMRI, multiparametric MRI; CheckDEEP, Checklist for DEtection of ExtraProstatic findings; T1w, T1-weighted; US, ultrasound; VI-RADS, Vesical Imaging–Reporting and Data System; VUJ, vesico-ureteric junction; ADC, apparent diffusion coefficient.

* Corresponding author.
E-mail address: andrea.ponsiglione@unina.it (A. Ponsiglione).
[1] The Authors equally contributed to the work.

https://doi.org/10.1016/j.ejrad.2023.110984
Received 29 May 2023; Received in revised form 10 July 2023; Accepted 16 July 2023
Available online 18 July 2023

anatomical structures can be recognized [7]. On one hand, a panoramic pelvic assessment guarantees PCa staging with the evaluation of prostate margins for extracapsular extension, seminal vesicle (SV) invasion, lymph nodes and adjacent organ involvement [8–10]; on the other hand, the workup prompted by IFs can result in patient anxiety and increased costs [11–13]. Thus, it is mandatory for a radiologist to be familiar with the various extra-prostatic findings potentially encountered during multiparametric MRI (mpMRI) reporting, which might impact patients' management [14]. In a previous study, Cutaia et al found the presence of IFs in more than half of their population, with the 2.6 % being clinically significant, thus requiring prompt treatment or impacting patient's prognosis [15].

With our pictorial review, we aim to illustrate a wide range of IFs that can be encountered when performing mpMRI of the prostate, classified according to anatomical structures and clinical relevance (Table 1).

Furthermore, we propose the CheckDEEP, the Checklist for DEtection of ExtraProstatic findings (Table 2), designed to detect additional findings outside the prostate gland. This checklist can be utilized both prior to and following the assessment of the prostate, allowing for a thorough evaluation of target areas within each anatomical system.

2. Extraprostatic findings

2.1. Genitourinary system

2.1.1. Not clinically significant

2.1.1.1. Seminal vesicle agenesis. SV agenesis is a rare anomaly with a reported incidence between 0.6 and –1 % [16] and may be unilateral or bilateral (Fig. 1a). Unilateral agenesis of the SV is thought to result from aberrant development of mesonephric duct before the seventh week of gestation (before separation of ureteric bud from the mesonephric duct), being associated with ipsilateral agenesis of kidney [17]. If the damage occurs after 7 weeks of gestation, the ipsilateral kidney will be present. Bilateral SV agenesis without associated urinary abnormalities is often seen in patients with cystic fibrosis due to luminal blockage of the SV and deferens vasa precursors from abnormal dense secretions during gestation. The main symptom associated with these conditions is infertility, although in most of the cases it is an incidental finding without prior clinical suspicion [18].

Table 1
Extraprostatic incidental findings according to anatomical structures and clinical significance.

System	*Not Clinically significant*	*Clinically significant*
Genitourinary	Seminal vesicle agenesia, stones, hemorrhage, and cyst; Cowper duct syringocele; penile prosthesis; spermatic cord hydrocele; epididymal cyst; testicular cyst; scrotolith; bladder stones and diverticulum; urachal cyst; ureterocele; ureteric stone	Seminal vesicle leiomyoma; bladder urothelial carcinoma
Gastrointestinal	Colonic diverticulosis; tailgut duplication cyst; hemorrhoids	Chron's disease; colorectal cancer; perianal abscess and fistula; colo-vesical fistula
Musculoskeletal	Inguinal hernia; iliopsoas bursitis; intramuscular lipoma; butterfly vertebra; Paget disease; osteoarthritis; femoral geodes	Sacrococcygeal chordoma; bone metastases
Neuro-vascular	Tarlov cyst; femoro-femoral bypass	Periprostatic schwannoma; pelvic arteriovenous malformation
Lymphatic	Pelvic lymphocele	Lymphadenopathy

Table 2
Checklist for DEtection of ExtraProstatic findings (CheckDEEP).

Target areas
Seminal vesicles
Bladder – Ureters
Rectum – colon – small bowel
Perirectal/presacral space
Pelvic vessels, lymphatics and nerves
Bones: hip, sacrum-coccyx, vertebrae, proximal femurs
Muscles: hip, pelvis, thigh
Inguinal canal
Inguinal vessels and lymph nodes
Scrotum – testis – penis
Perineum

2.1.1.2. Seminal vesicle stones. SV stones represent a rare entity and have been mainly reported after the age of 40 years [19]. They can be asymptomatic or manifest with hematospermia, hematuria, dysuria pelvic, perineal, testicular, ejaculatory pain and rarely spermolithiasis. The etiology of SV calculi remains unclear; however, they could be associated with various genitourinary inflammatory processes, diabetes mellitus, hyperparathyroidism, and congenital anomalies. On MRI, they appear as intraluminal structures, characterized by low T2w signal, without diffusion restriction or enhancement (Fig. 1b) [20].

2.1.1.3. Seminal vesicle hemorrhage. Abnormal signal intensity of the SV has been observed in 1.7 % of screening population, mostly without any clinical significance [21]. Normal appearances of the SV are grape-like clusters with high T2 signal intensity of internal fluid and low T2w signal intensity of the wall. Due to the heterogeneous composition of the fluid, it is not unusual to find various degrees of weak hyperintensity on T1w images. However, fluid with only a high concentration of protein and mucin is unlikely to show signal intensity higher than fat on T1w. On these cases, hyperintensity content on T1W is usually related to hemorrhage especially in patients with clinical hematospermia (Fig. 1c–d) [22]. Causes of hemorrhage within the SV include obstruction (cysts or calculi), urogenital infections, trauma, chronic abstinence, tumors, and systemic conditions (e.g., bleeding diatheses, lymphoma and amyloidosis) [23].

2.1.1.4. Seminal vesicle cyst. SV cysts are a rare IF on prostate mpMRI (incidence about 0.005 % of the population) that can be congenital or acquired [24]. Congenital cysts are usually encountered in patients between the 2nd and 3rd decade of life and can be isolated or, more often, associated with upper urinary tract anomalies, such as autosomal dominant polycystic kidney disease or ipsilateral renal dysgenesis, like in Zinner syndrome (Fig. 2) [25]. This latter is a developmental anomaly of Wolffian duct, characterized by the triad of renal agenesis, ejaculatory duct obstruction and seminal vesicles' cysts. Acquired SV cysts are most often seen in elderly patients. Small SV cysts are usually asymptomatic, while large SV cysts (greater than 5 cm) manifest symptoms during the period of greatest reproductive activity. Patients with SV cysts may present with chronic recurrent prostatitis, epididymitis, painful ejaculation, hematuria/hematospermia, infertility, perirectal or pelvic discomfort and/or perineal or testicular pain. The classical cystic appearance is maintained, with low T1w and high T2w signal intensity; variable increased T1 signal is seen with increasing haemorrhagic or proteinaceous cyst content.

Various pathologic conditions can arise in or around the SVs and mimic SV cysts, including obstruction of the SV, vas deferens or ejaculatory ducts, or conditions such as dilated ectopic ureter and ureterocele [24]. If symptomatic, an ultrasound (US)-guided drainage can be resolutive.

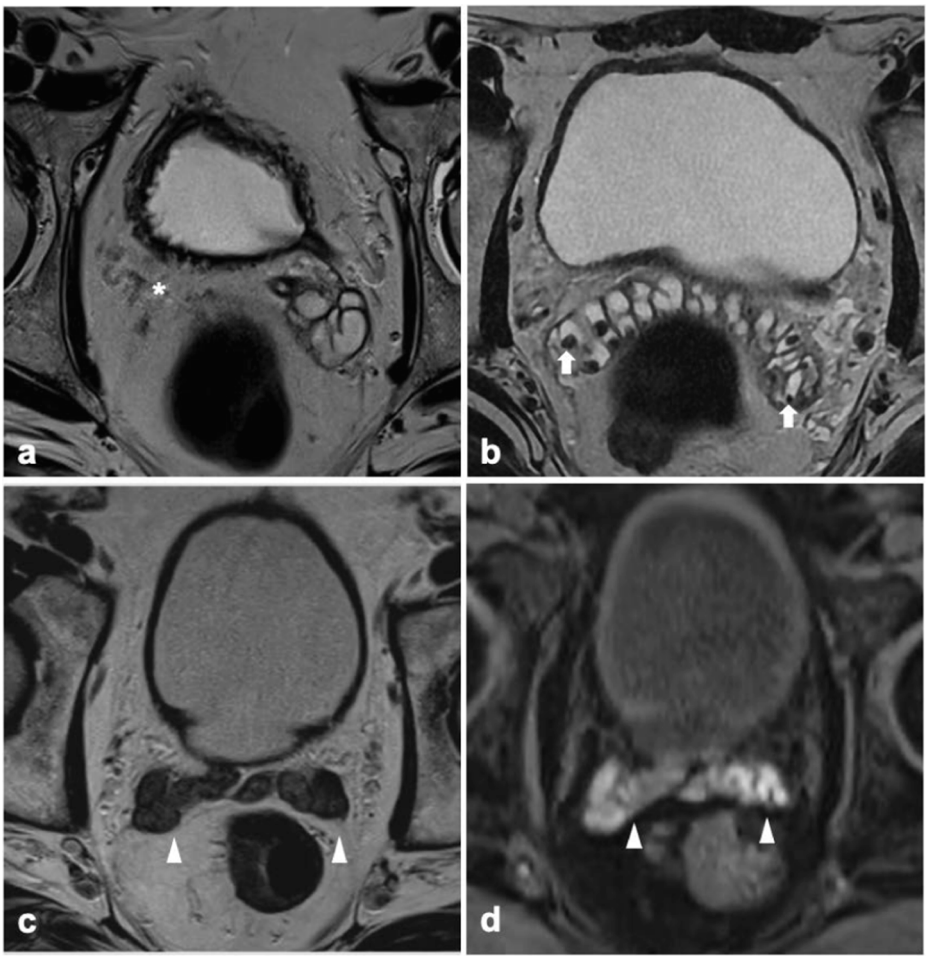

Fig. 1. Axial T2w image (a) documents agenesia of the right seminal vesicle (asterisk). Axial T2w image (b) shows multiple rounded hypointense structures in both the seminal vesicles (arrows), in keeping with calculi. Axial T2w (c) and pre-contrast fat-sat T1w (d) images show respectively hypointense and hyperintense signal within both the seminal vesicle (arrowheads), findings suggestive of blood content. *T2w* T2-weighted, *T1w* T1-weighted.

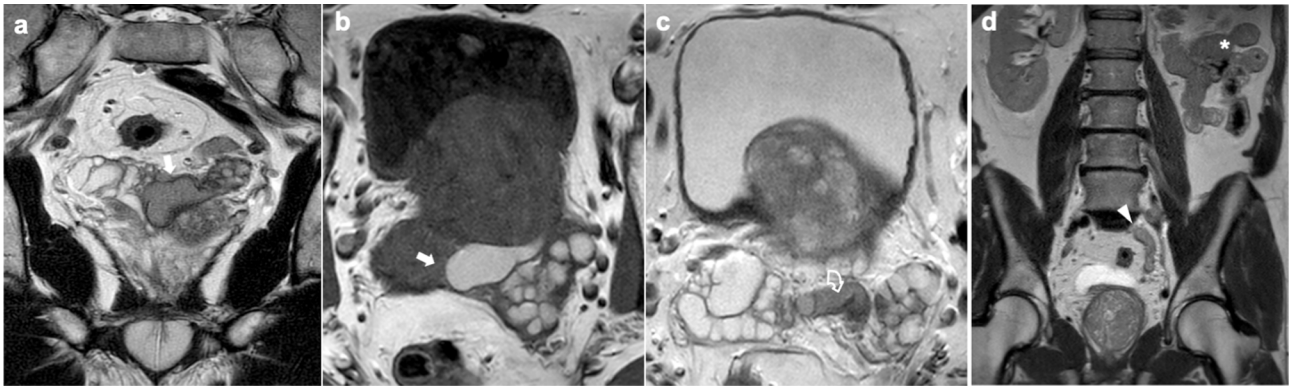

Fig. 2. Coronal T2w (a) and axial T1w images (b) show a left unilateral cyst of the seminal vesicle with protein content (arrows), while axial T2w image (c) depicts ectasia of the left vas deferens with inhomogeneous content (curved arrow). Coronal large FOV T2w image (d) of the same patient shows ipsilateral renal agenesis (asterisk) and the ureteral embryonic residual (arrowhead). The findings are consistent with Zinner syndrome. *T2w* T2-weighted, *T1w* T1-weighted, *FOV* field of view.

2.1.1.5. Cowper duct syringocele. A Cowper duct syringocele is a congenital or acquired dilatation of the Cowper gland's duct in the bulb of the corpus spongiosum. Symptoms include lower urinary tract symptoms, such as frequency, urgency, dysuria, weak stream, post-void incontinence, recurrent urinary tract infections and hematuria; occasionally a painful perineal mass is reported [26]. Clinical signs are frequently related to the degree of duct dilatation and whether the syringocele communicates or not with the urethra. Indeed, open syringocele is more related to post-void incontinence, whereas closed syringocele is related to infravesical obstruction.

On MRI, it appears as midline fluid-filled formations located at the ventral aspect of the bulb of the corpus spongiosum (Fig. 3a–b). Four

Fig. 3. Sagittal (a) and coronal (b) T2w images show a hyperintense midline unilocular cystic lesion at the penile base close to the proximal bulbous urethra, in keeping with Cowper's gland syringocele. Coronal (c) and sagittal (d) T2w images show paired T2-hyperintense cylinders in the corpora cavernosa (arrowheads), a left-side pelvic fluid-filled reservoir (asterisk) and a hypointense rear tip extender (star) of a well-placed three-piece IPP. *T2w* T2-weighted, *IPP* Inflatable penile prosthesis.

imaging types of syringocele have been described: simple, perforated, imperforated and ruptured [26]. Imperforated syringocele is easily diagnosed as it presents as a submucosal cyst with low T1w and high T2w signal.

The remaining three types are difficult to distinguish as they differ only in the degree of dilatation of the bulbourethral duct and the grade of communication with the urethral lumen [27].

2.1.1.6. Penile prosthesis. Penile prostheses, also named penile implants, represent the surgical treatment option for irreversible organic erectile dysfunction [28]. Currently, two types of implants are available: the malleable ones, consisting of two paired semi-rigid rods that are surgically placed in each of the corpora cavernosa, and the inflatable ones. The latter may be of three-pieces or two-pieces type. In detail, the three-piece inflatable penile prosthesis consists of two inflatable cylinders that are placed within the corpora cavernosa, a pump within the scrotum, and a reservoir located close to the bladder, generally filled with normal saline. On MRI, the inflatable cylinders are homogeneously T2w-hyperintense due to their saline content, while the silicone-based covering of the cylinders is T2w-hypointense (Fig. 3c–d). The proximal segment of the cylinders, named as rear tip extender, appears thinner and hypointense on T2w images. Scrotal control pump appears as an oval shaped T2w hyperintense structure with a metallic artifact caused by its valve apparatus while the pelvic reservoir consists of a round or oval structure hyperintense on T2w sequence. All three components are connected by thin silicone tubing, which appears as a T2-hypointense tubular structure [29]. Possible complications of cylinders include aneurysmal dilatation, migration, kinking and crossover, while rupture and migration should be excluded for both the reservoir and the pump.

2.1.1.7. Spermatic cord hydrocele. Spermatic cord hydrocele consists of a collection of fluid along the spermatic cord not communicating with the scrotal sac. Embryologically, it results from an abnormal defect in the closure of the processus vaginalis [30].

On MRI, it appears as a fluid collection, with a high signal on T2w and subtle wall enhancement, separated from the testis and communicating with the peritoneal cavity at the level of internal inguinal ring (Fig. 4a–b) [31]. It should not contain any bowel loop or vascularity. The main differential diagnoses include indirect inguinal hernia, which may contain bowel loops, vascularity or even a bladder portion, and scrotal hydrocele.

2.1.1.8. Epididymal cyst. Cysts are the most common epididymal masses, reported in 20–40 % of asymptomatic individuals [32]. They may be true simple cysts or retention cysts. Simple cysts originate from the lymphatic ducts and are provided with epithelium cells containing a clear serous liquid, whereas retention cysts are caused by dilated tubules in response to inflammatory or congenital obstruction of the seminiferous tubules. Their content is usually corpuscular and dense because it is formed by sperm, protein, white blood cells and cell exfoliation. These cysts may become quite large (5 cm in diameter) and develop in the vaginal cavity, in which case they are called spermatoceles. On MRI, they appear as well-defined high-T2w, low-T1w signal lesions, occasionally showing internal septations, and typically located in the epididymal head (Fig. 4c) [33].

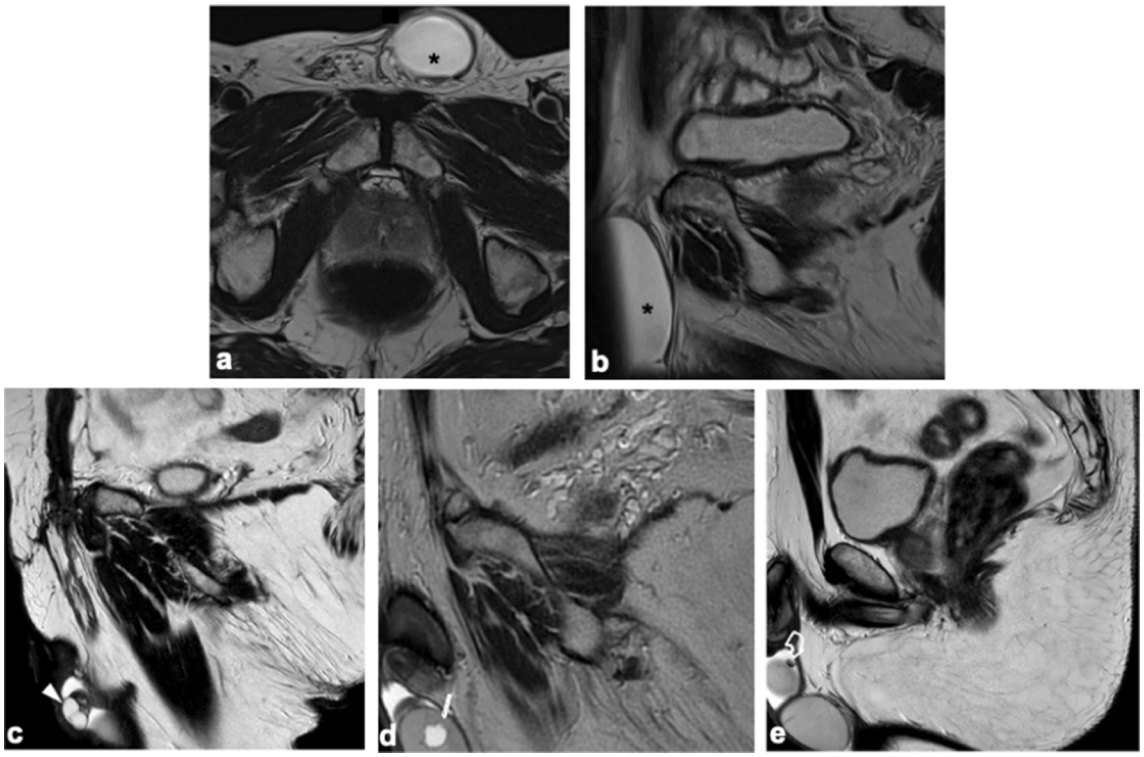

Fig. 4. Axial (a) and sagittal (b) T2w images show a fluid collection (asterisks) along the spermatic cord that lies superior to the testicle and does not communicate with the scrotal sac, in keeping with spermatic cord hydrocele. Sagittal T2w image (c) shows two small cysts of the epididymal head (arrowhead). Sagittal T2w image (d) shows a small rounded simple testicular cyst (arrow). Sagittal T2w image (e) shows left hydrocele containing a small low signal rounded lesion (curved arrow), consistent with scrotolith. *T2w* T2-weighted.

2.1.1.9. Testicular cyst. Simple cysts are often found incidentally on US, but occasionally also on MRI. They have typical features: thin wall, liquid content, and well-defined margins (Fig. 4d) [34]. Their etiology is unclear, but they may occur after trauma or inflammation. They are usually single with a variable size (2–20 mm), intratesticular-located close to the mediastinum and do not require surgical treatment. Simple testicular cysts should be carefully differentiated from cystic neoplasms, such as cystic teratoma whose mass is often palpable and large requiring surgical treatment. Moreover, intratesticular spermatocele as well as intratesticular varicocele represent other differential diagnoses [35].

2.1.1.10. Scrotolith. Scrotoliths (also called scrotal pearls) are rare extra-testicular calcifications, incidentally found in about 3 % of the general male population [36]. Scrotolith's exact aetiology is unclear. Possible causes are linked to inflammation and resultant fibrosis of the tunica vaginalis, infections by parasites (filarial), appendix testis or epididymis torsion which subsequently calcifies, and chronic microtrauma [37]. The scrotoliths can be single or multiple and usually range in size from a few mm up to 1 cm, therefore being clinically impalpable. On MRI they can be detected as signal voids on conventional T1w and T2w sequences, surrounded or not by a T2w hyperintense hydrocele (Fig. 4e). Scrotal pearls are benign lesions and not require any treatment or follow-up.

2.1.1.11. Bladder stones. Bladder stones represent only 5 % of all urinary tract calculi [38].They can be categorized as primary (in the absence of other urinary tract abnormality, typically seen in children in endemic areas), secondary (due to urinary stasis or from concretions on foreign bodies such as Foley catheters) and migratory (related to the migration of a renal stone). The most frequent cause of bladder stones is urinary stasis in conditions such as benign prostatic hyperplasia or neurogenic bladder disorder. Other predisposing factors include radiation therapy, schistosomiasis, bladder augmentation surgery, urethral strictures, and the presence of bladder diverticula. Symptoms might be absent, related to an incomplete bladder emptying, or non-specific such as terminal hematuria, suprapubic pain, weak stream, and dysuria.

On mpMRI, they appear as rounded T1w and T2w signal voids located into the urinary bladder in a gravity-dependent position (differently from intravesical gas that might have similar MRI signal but anti-gravity position), surrounded by the hyperintense urine on T2w images (Fig. 5a) [39]. Despite dissolution of stones can be sometimes accomplished with oral alkalinizing agents, in most of the cases they are managed with endoscopic or open surgery, depending on their dimensions [40].

2.1.1.12. Bladder diverticulum. Bladder diverticulum is defined as the outpouring of the mucosa through the points of least resistance of the muscular layer. If the acquired form is the most common to be found in the adult population, the congenital form is rare and recognizable occasionally during diagnostic investigations for lower urinary tract symptoms [41]. The secondary diverticula are generally multiple and originate from obstructive causes, while the congenital form is single and located postero-medially to the ureteral meatus due to a congenital anomaly of the muscle fibers. Moreover, the congenital form has all the layers of the wall although the muscularis propria appears thinned, while the secondary ones lack the muscular layer. If the congenital diverticulum presents within the orifice of the ureteral meatus, the diverticulum is called "Hutch's diverticulum" (Fig. 5b) [42].

Diverticula may be associated with several complications due to urinary stasis: infection, transient intra-diverticular cell carcinoma (1–10 %), bladder stones and bladder rupture.

2.1.1.13. Urachal cyst. Urachal cysts represent one of the manifestations of the spectrum of congenital urachal remnant abnormalities [43].

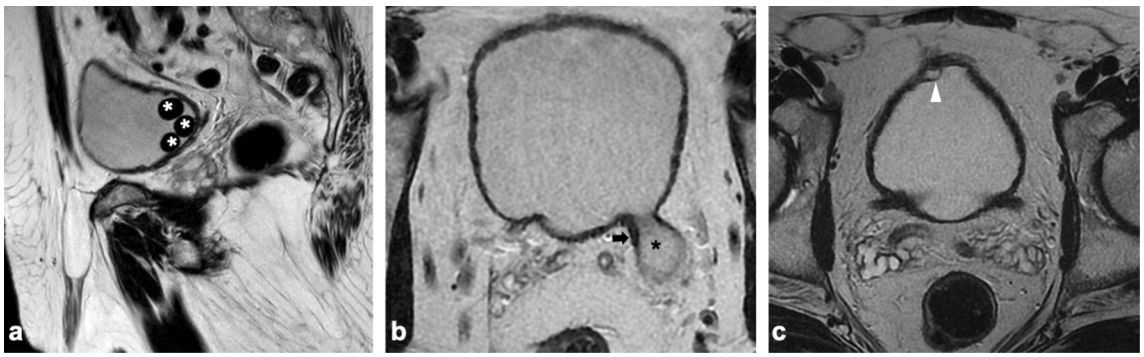

Fig. 5. Sagittal T2w image (a) shows multiple intraluminal signal voids (white asterisks) within the hyperintense fluid in the urinary bladder, in keeping with stones. Axial T2w image (b) shows a bladder diverticulum (black asterisk) involving the left ureteral meatus (black arrow), known as Hutch diverticulum. Axial T2w image (c) shows a well-capsulated homogenous fluid-filled structure (arrowhead), adjacent to the bladder apex, at the attachment of the median umbilical ligament, consistent with urachal cyst. *T2w* T2-weighted.

They occur when the urachus closes at both ends (bladder and umbilicus) but remains open between the two extremities, more frequently in the lower third, in the closeness of the urinary bladder. Usually, the urachal cysts are small and asymptomatic. On MRI, when uncomplicated, they appear as thin-walled homogenous, T1w hypointense, T2w hyperintense, cystic lesions without diffusion restriction or enhancement on DCE sequences (Fig. 5c) [44]. Infection, bleeding, wall calcifications as well as the rupture into the peritoneal cavity may represent possible complications.

2.1.1.14. Ureterocele. Ureteroceles are saccular dilatations of the intramural course of the ureter, secondary to an abnormal congenital obstruction of the ureteral meatus. The most accepted pathogenetic theory is a failure in the regression of an embryologic membrane around the distal ureter [45]. They occur most commonly in the Caucasian population, in about 1 in 4000 children and there is a 4–7:1 female-to-male ratio. Ureteroceles may be associated with a duplicated (80 % of cases) or single collecting system and categorized as either orthotopic (i.e., occurring at the expected vesico-ureteric junction -VUJ- position), mostly in adult age, or ectopic (i.e., occurring outside of the expected VUJ, in an extravesical site such as the urethra or vagina), much more common in children. Ureteroceles vary in size from less than a centimeter to a large structure that fills the entire bladder and might be bilateral in about 10 % of cases [46]. They can be asymptomatic or manifest in relation to VUJ obstruction and reflux with urinary tract infections, urosepsis, frequency, hematuria, pain, urinary retention, and

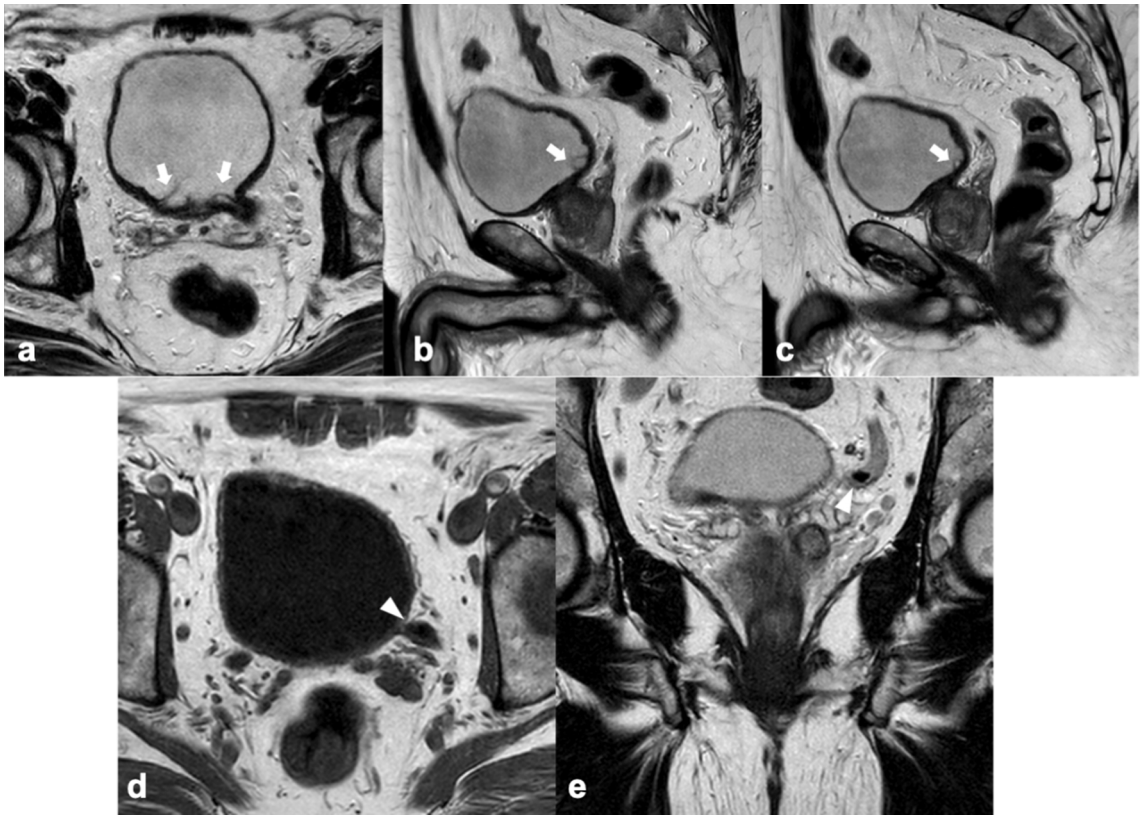

Fig. 6. Axial (a) and sagittal T2w images (b-c) show bilateral cystic dilatation of the terminal ureter at its opening into the bladder (arrows), in keeping with ureterocele. Axial T1w (d) and coronal T2w (e) images show a dilated left ureter with a juxta-vesical hypointense stone (arrowheads). *T2w* T2-weighted, *T1w* T1-weighted.

stone disease. They appear as an intravesical cystic structure continuous with the distal ureter showing the typical "cobra head sign", best seen on the T2w sequences (Fig. 6a–c). In such cases an additional heavily T2-weighted (urographic) scan might be performed to better display the whole urinary tract. Ureterocele may prolapse into the ureter or the urethra depending on the position, causing acute complete urinary obstruction. When symptomatic, treatment of the ureterocele is recommended and consists in control of infections and endoscopic or surgical repair [47].

2.1.1.15. Ureteric stones. Ureteric stones may be encountered within the course of the ureter, at any point from the ureteropelvic junction to the VUJ. They more frequently occur in men, with peak incidence between ages 35–45 [48]. Patients with ureteric calculi generally present with peristaltic pain, nausea, hematuria and vomiting. Calculi located in the VUJ may also manifest with irritative symptoms such as dysuria and urinary frequency. On MRI, they appear as intraluminal structures, hypointense on T2w images, without diffusion restriction or enhancement on DCE sequences (Fig. 6d–e) [49]. The location, size, and shape of the stone are all important factors in determining the best treatment option. Analgesics, extracorporeal shock wave lithotripsy, ureteroscopic lithotripsy, and laparoscopic ureterolithotomy represent therapeutical options for ureteral stones.

2.1.2. Clinically significant

2.1.2.1. Seminal vesicle leiomyoma. Primitive neoplastic diseases of SV are rare and there are only a few case series in the literature, mainly describing benign solid tumors such as cystadenoma, leiomyoma, schwannoma and paraganglioma [50,51]. Malignant tumors include intraepithelial neoplasia, adenocarcinoma, leiomyosarcoma, rhabdomyosarcoma and squamous cell carcinoma. Their imaging features are heterogeneous, and their distinction requires always histological confirmation [52]. Among benign tumors, leiomyomas are the most represented and should be considered when approaching a solid mass arising from SV without evidence of PCa. They are benign smooth muscle cell tumors of monoclonal origin and may arise from almost every part of the genitourinary system. Patients with leiomyoma of SV are often asymptomatic, although irritative symptoms and infertility may occur [51]. Typically, leiomyomas appear as oval-shaped masses, well-circumscribed, with low signal intensity on T2w (because of high collagen content), iso-intense on T1w images, with intense enhancement on DCE (Fig. 7).

2.1.2.2. Bladder urothelial carcinoma. Bladder cancer is the second most common genitourinary malignancy after prostate cancer. Ninety percent of cases are urothelial subtypes, and up to 70 % of them present as non-muscular invasive bladder cancer, which has a better prognosis than the muscular-invasive counterpart [53].

Among radiological evaluations, MRI has a high diagnostic performance in evaluating the invasion of the muscular layer, improving the accuracy for diagnosis of the primary and recurrent tumor and monitoring response to treatment [54]. Tumors usually appear as either sessile or papillary projections from the wall, with intermediate-to-high signal intensity on T2w, restricted diffusion, and early enhancement after contrast administration (Fig. 8). The paramount role of radiology is disease staging. Whether a further dedicated MRI bladder is performed, it is possible to evaluate if muscular invasion (T1 vs T2), perivesicular, (T3), or extension to the adjacent tissues (T4) would be present. The Vesical Imaging–Reporting and Data System (VI-RADS) score has been recently proposed and validated to differentiate muscle-invasive versus non-muscle-invasive bladder cancer [55,56].

2.2. Gastrointestinal system

2.2.1. Not clinically significant

2.2.1.1. Colonic diverticulosis. Diverticular disease has become more common over the last century. Autopsy studies from the early 20th century reported colonic diverticula rates ranging from 2 % to 10 %. This has risen dramatically over time. Diverticular disease has traditionally been thought to be a disease of the elderly with prevalence of up to 65 % by 85 years of age and is estimated to be as low as 5 % in those 40 years of age or younger [57]. Colonic diverticulosis manifests as distinctive colonic, sac-like outpouchings, most commonly affecting the sigmoid colon in left-sided disease (Fig. 9a). It is critical to define the location, severity, and presence of complications in order to properly manage patients, as most patients with mild disease can usually be successfully treated medically [58]. Colonic diverticulitis represents a complication of colonic diverticulosis. Symptoms of colonic diverticulitis generally arise from the left iliac fossa with unremitting pain and accompanying tenderness. The MRI diagnosis of colonic diverticulitis is based on the presence of bowel wall thickening, pericolonic stranding and the presence of diverticula [59]. Complicated diverticulitis may manifest with phlegmon or small abscess formation, perforation and even fistulation with contiguous organs.

2.2.1.2. Tailgut duplication cyst. Tailgut duplication cyst represents a cystic lesion located in the retrorectal or presacral space, probably arising from vestiges of an embryonic hindgut [60]. While it can present at any age, they more frequently manifest between 30 and 60 years. Almost 50 % of patients may show perirectal symptoms, such as pelvic pain and constipation. Most cases present either as a multilocular or a unilocular cystic lesion, with high T2 signal intensity and variable T1 signal intensity according to the variable amount of contained proteinaceous material (Fig. 9b).

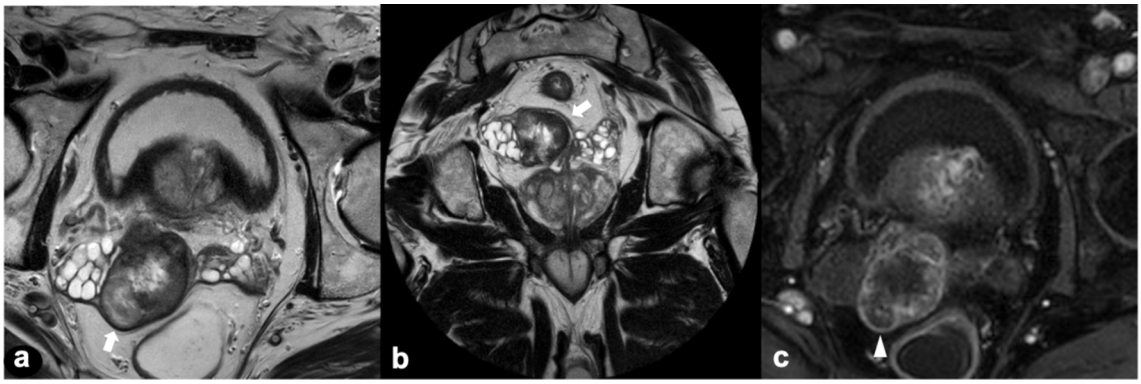

Fig. 7. Axial (a) and coronal T2w (b) images show a heterogeneous encapsulated mass arising from the right seminal vesicle, with cystic and solid components (arrows) and with inhomogeneous enhancement on DCE image (arrowhead). Biopsy revealed leiomyoma. *T2w* T2-weighted, *DCE* dynamic contrast enhanced.

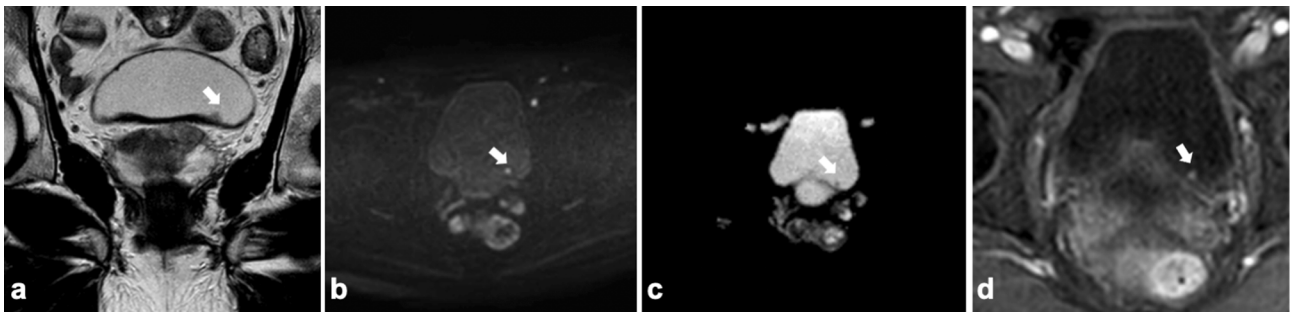

Fig. 8. Small intraluminal bladder lesion adhered to the left posterior wall (arrows) hypointense on coronal T2w image (a), hyperintense on axial high-b value DWI (b), hypointense on ADC map (c) with early enhancement on DCE image (d), confirmed as a non-muscle invasive urothelial carcinoma at the histopathological examination. *T2w* T2-weighted, *DWI* diffusion weighted imaging, *ADC* apparent diffusion coefficient, *DCE* dynamic contrast enhanced.

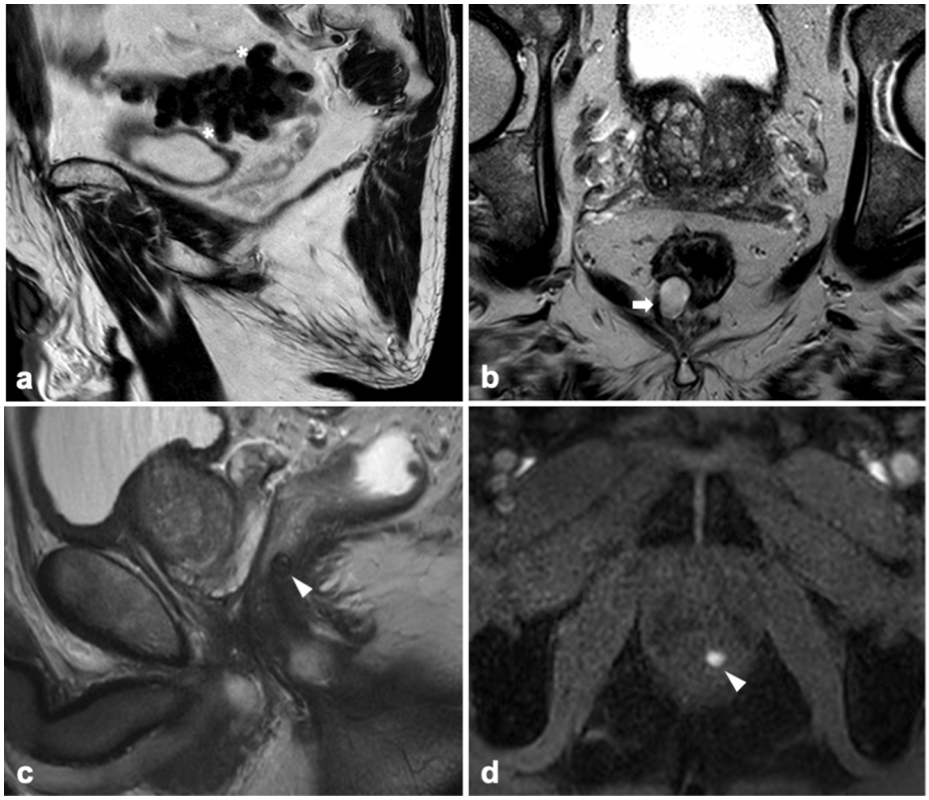

Fig. 9. Sagittal T2w image (a) shows multiple diverticula of the sigmoid colon (asterisks), in keeping with diverticulosis, without signs of diverticulitis. Axial (b) T2w images show a cystic lesion in the presacral space indenting posterior rectal wall (arrow), in keeping with Tailgut duplication cyst. Sagittal T2w (c) and axial fat-sat T1w (d) images show a T2-hypointense and T1-hyperintense rounded lesion in the rectum (arrowheads), consistent with thrombosed internal haemorrhoid. T2*w* T2-weighted, *T1w* T1-weighted.

The differential diagnoses include other benign cystic masses such as cystic lymphangioma (also multilocular), epidermoid, dermoid, duplication cysts as well as anterior meningocele, all of which are usually unilocular [61].

2.2.1.3. Hemorhoids. Hemorrhoids are submucosal sinusoids that act as vascular cushions in the anal canal and are ubiquitous in the adult population [62]. Depending on whether they are located, above or below the dentate line, they are classified as internal or external hemorrhoids, respectively. Abnormal dilatation of these subepithelial cushions causes "hemorrhoidal disease", characterized by rectal bleeding, mucous-like discharge, pruritus and discomfort. In the case of acutely thrombosed hemorrhoids, severe pain may occur. Although the diagnosis is clinical, given the vast prevalence in the population, hemorrhoids are not an uncommon incidental finding in patients referred to MRI for PCa suspicion. Non-thrombosed hemorrhoids have generally a high signal intensity on T2w images, with enhancement on delayed dynamic phase (Fig. 9c–d). Thrombosed hemorrhoids are often less intense on T2w imaging and have a slightly thicker wall with surrounding inflammation, thereby mimicking an abscess [63]. Treatments range from non-operative management to sclerotherapy, coagulation, and banding or, in case of severe disease or previous therapies failure, surgical hemorrhoidectomy [64].

2.2.2. Clinically significant

2.2.2.1. Crohn's disease. Crohn's disease is a disorder of the spectrum of inflammatory bowel disease, a chronic idiopathic process characterized by transmural inflammation at any location of the gastrointestinal tract, predisposing patients to fistulas and strictures. The most involved location is the terminal ileum [65]. Chron's disease generally manifests between the ages of 15 and 25 years without gender predilection. Patients usually present with chronic diarrhea and recurrent abdominal pain, however in a few cases the presentation occurs as a complication or an extraintestinal manifestation. The disease features are those of an inflammatory process, either in the acute or chronic phase. The acute

inflammatory findings include bowel wall thickening (more than 3 mm) with high-signal intensity on T2w sequences and post-contrast enhancement, as well as prominent vasa recta ("comb sign"), mesenteric fat stranding, and enlarged mesenteric lymph nodes (Fig. 10) [66]. On the contrary, in the fibrostenotic phase, the signal intensity on T2w is usually low. The common complications are sinus tracts, fistulae and bowel obstruction, either from active inflammation or fibrostenotic disease.

2.2.2.2. Colorectal cancer. Colorectal cancer is the third most common cancer in men and the second most common in women, with the highest prevalence in the most developed countries (Fig. 11). The risk factors are related to family and personal medical history (e.g. colon polyps, inflammatory bowel disease), lifestyle (e.g. obesity, red meat intake, cigarette smoking) and genetic conditions (e.g. familial adenomatous polyposis coli and its variants, Lynch-associated syndromes) [67]. Common reported symptoms are rectal bleeding, abdominal pain, change in bowel habit, weakness, unexplained weight, and appetite loss; however, patients can be also asymptomatic and presenting in an advanced stage with an intestinal occlusion [68]. Currently, rectal MRI is considered the imaging modality of choice for rectal cancer local staging [69]. During prostate mpMRI, rectal cancer can be incidentally detected as a polypoid, annular or semi-annular lesion with intermediate signal on T2w sequences, showing restricted diffusion on high b value DWI and on apparent diffusion coefficient (ADC) maps. Location (low-, medium-, high-rectum, sigmoid colon), length, distance from the anorectal angle or the anal verge, rectal wall layers involvement, infiltration of the perirectal fat, extramural vascular invasion, distance from the meso-rectal fascia, anal sphincter invasion, involvement of the peritoneal folds and contiguous organs or structures, should be always reported. Nodal local staging should be also performed (dimensions, margins and internal inhomogeneities are the features considered for the nodal involvement). Recto-colonoscopy is mandatory to confirm the diagnosis and to identify synchronous or metachronous lesions. The treatment (surgery, neoadjuvant chemoradiotherapy, chemoradiotherapy alone) should be always discussed in a multidisciplinary environment.

2.2.2.3. Perianal abscess and fistula. Perianal abscesses are infective-inflammatory collections that may have different origins. They can be isolated and generally originate from an obstruction of the anal glands (cryptoglandular theory) or may be associated with fistulas or chronic inflammatory bowel disease. Pelvic-perineal pain is often the main symptom with swelling area. Based on the anatomical relationships with the muscular structures of the pelvis, abscesses can be distinguished into 4 groups with different incidence: superficial perianal (43 %), ischioanal (23 %), intersphincteric (21 %), supralevator muscle (7 %) [70]. The treatment is surgical, with incision and drainage of the abscess. MRI represents the technique of choice for the study of pelvic anatomy, allowing to provide an appropriate classification of abscesses with or without fistulas. T2w sequences enable to visualize the fluid content of both the abscess and fistulas as hyperintense in an acute phase, while T1w and T2w signal hypointensity suggests chronicity of the findings (Fig. 12). The use of intravenous contrast agent helps to distinguish an acute phase fistula (wall enhancement) from a healing phase (diffuse enhancement also at the lumen level from granulation tissue) [71]. Some Authors suggested that DWI is even more sensitive than T2w images in identifying fistula and could represent an alternative to post-contrast imaging [72].

2.2.2.4. Colo-vesical fistula. Colo-vesical fistula consists of a communication between the lumen of the colon and the bladder, which may be direct or via an intervening abscess cavity. It represents an unusual complication of a wide range of pathologies, first of all, diverticular disease followed by inflammatory bowel disease, colon and bladder cancers as well as radiotherapy [73]. Rare causes are represented by appendicitis and trauma. Faecaluria is a late but pathognomonic sign while pneumaturia is suggestive of colo-vesical fistula if clinically suspected. Many cases present with non-specific signs and symptoms such as recurrent urinary tract infections, dysuria or hematuria, which may delay diagnosis. Due to the inherent contrast of the fistula's fluid contents and its wall, MRI can demonstrate fistula morphology and anatomical location. Fistula appears as a linear track, hyperintense on T2w and isointense on T1w sequences, communicating between the two organs, with restricted diffusion and wall enhancement after intravenous contrast injection (Fig. 13). Free fluid, lymph nodes enlargement, fat stranding and an intervening abscess may be encountered [74].

2.3. Musculoskeletal system

2.3.1. Not clinically significant

2.3.1.1. Inguinal hernia. An increase in intra-abdominal pressure can lead to the development of abdominal hernias, with 75–80 % of them being inguinal. The causes can be different, for example, a chronic cough, obesity and ascites or they can arise after abdominal surgery [75]. The clinical picture generally allows diagnosis, with patients reporting an inguinal mass growing in size or appearing with cough and after Valsalva maneuver. However, the diagnosis may also occur incidentally during radiological examinations. Inguinal hernias are classified as direct (defect in the posterior wall of the inguinal canal) placed medially to the lower epigastric vessels, or indirect (the content passes

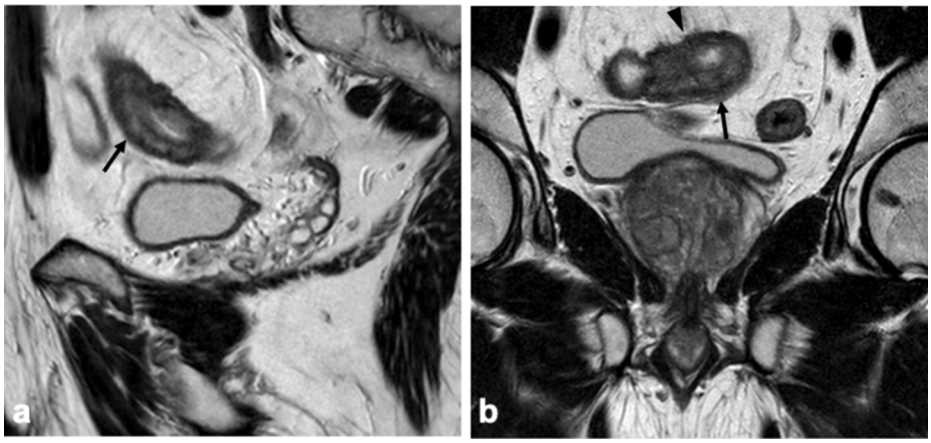

Fig. 10. Sagittal (a) and coronal (b) T2w images show terminal ileum wall thickening (arrows). Note the fibrofatty proliferation and the comb sign (arrowhead in b); Crohn's disease was then confirmed. *T2w* T2-weighted.

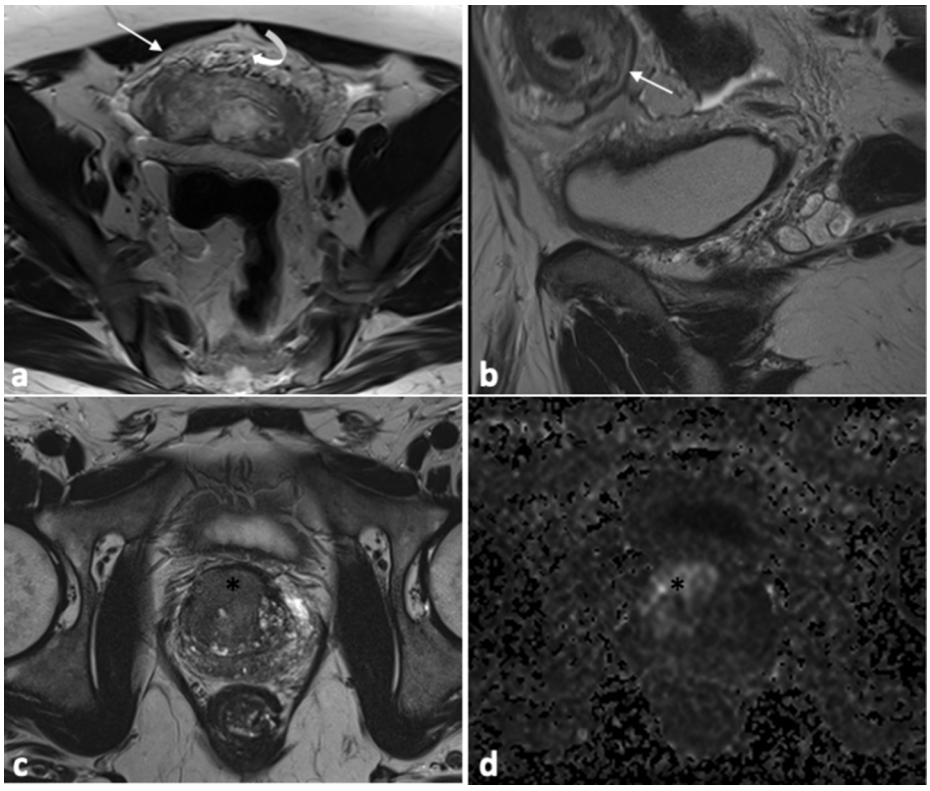

Fig. 11. Axial (a) and sagittal T2w (b) images show a sub stenosing sigmoid lesion (arrows) with fat stranding (curved arrow), pathologically confirmed after Hartmann's procedure as mucinous carcinoma with traits of signet ring cells. The same patient shows a PI-RADS 5 transitional zone prostatic lesion (asterisks) hypointense on axial T2w image (c) and hyperintense on axial high-b value DWI (d), confirmed at target biopsy as clinically significant prostate cancer (Gleason 8) with aspects of signet ring cells. *T2w* T2-weighted, *DWI* diffusion weighted imaging.

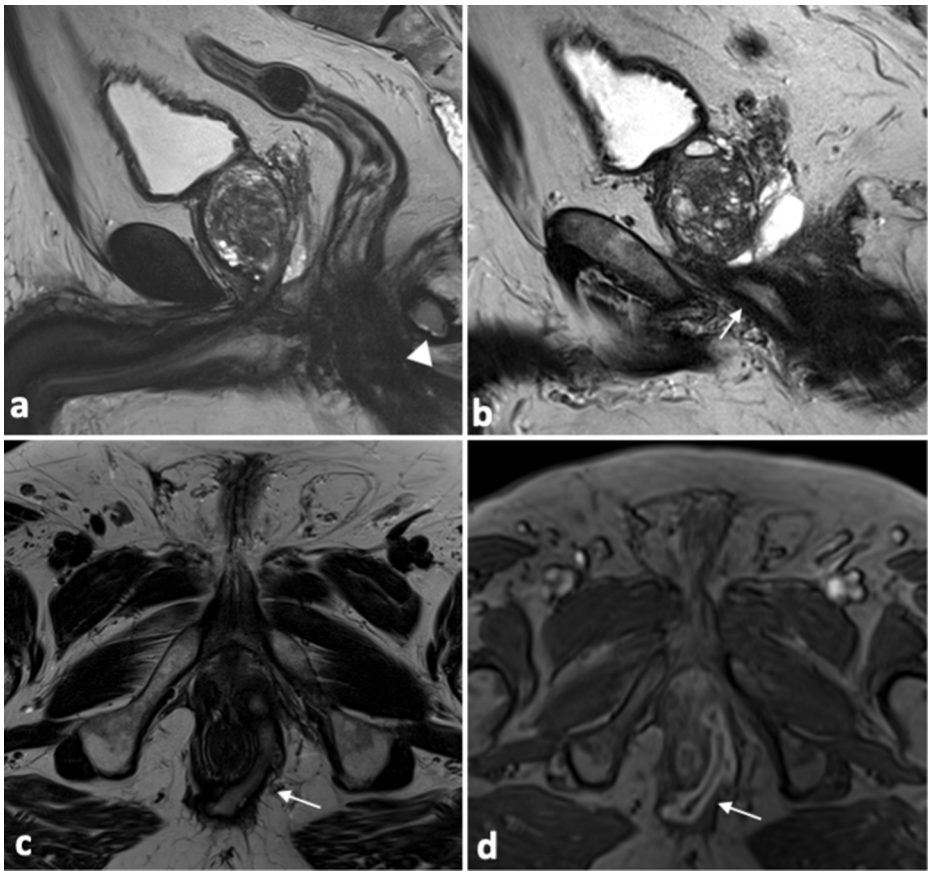

Fig. 12. Midline sagittal T2w image (a) shows a perianal abscess (arrowhead), while left paramedian sagittal (b), axial (c) T2w images and axial DCE image (d) show inter-sphincteric and *trans*-sphincteric fistulous tracts towards the prostate (arrows). *T2w* T2-weighted, *DCE* dynamic contrast enhanced.

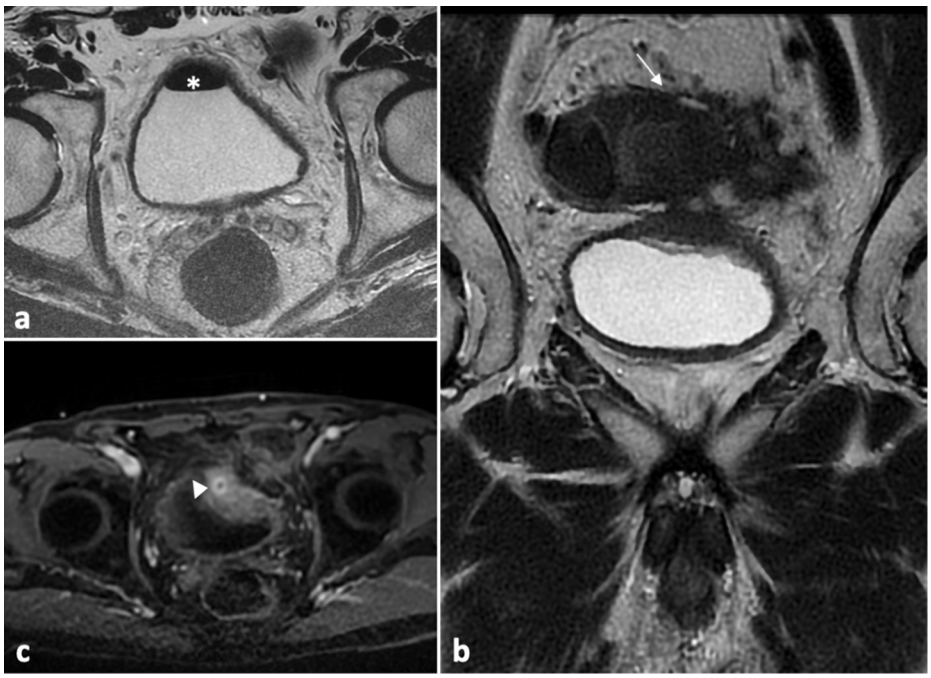

Fig. 13. Axial (a) and coronal (b) T2w images show gas within the bladder (asterisk) secondary to diffuse thickening of the sigmoid colon wall (arrow) with an enhancing fistulous connection towards the bladder depicted on axial DCE image (arrowhead in c), in keeping with colo-vesical fistula. *T2w* T2-weighted, *DCE* dynamic contrast enhanced.

through the deep ring in the canal) placed laterally to the lower epigastric vascular-nervous bundle. US represents the first line imaging technique for diagnosis, while computed tomography (CT) is used in case of acute pain, often a sign of complications (occlusion and/or perforation of a bowel). MRI could be useful in cases of dubious inguinal hernia in order to identify potential differential diagnoses such as femoral hernia, hydrocele or muscle trauma (Fig. 14a–b) [76]. It is essential to report the site and the three components of the hernia, namely the sac, the neck, and the contents. The latter is usually mesenterial adipose tissue and/or an intestinal loop, but it is not uncommon to also find retroperitoneal viscera such as the bladder.

2.3.1.2. Iliopsoas bursitis. Iliopsoas bursa interposes between the iliopsoas tendon and the articular capsule of the hip joint, and it is not

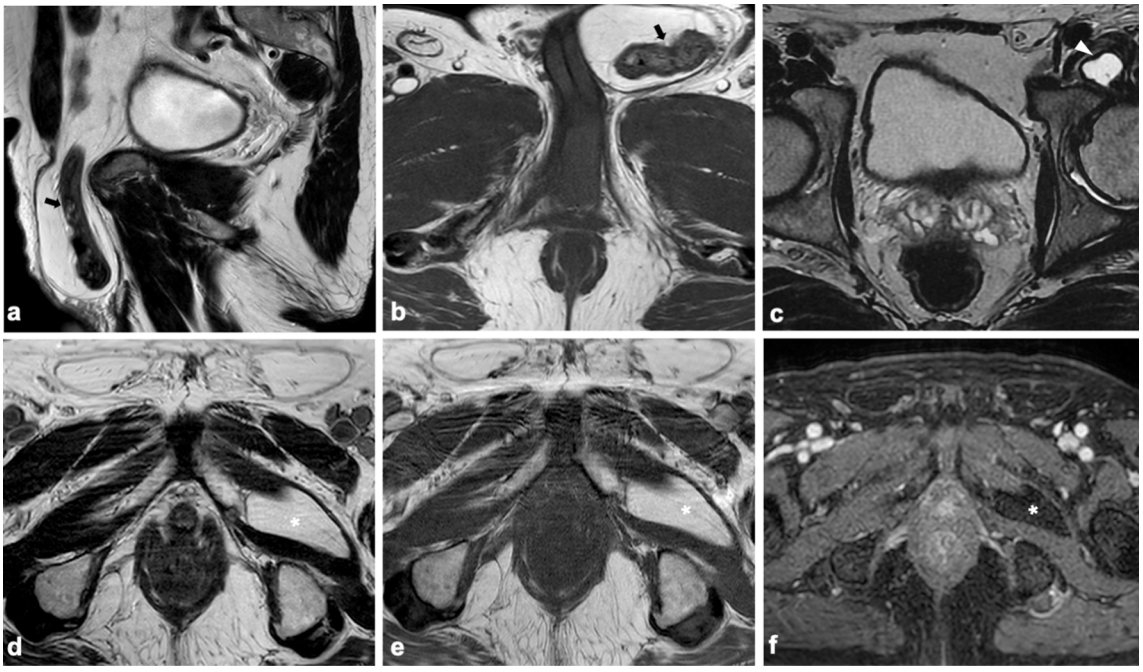

Fig. 14. Sagittal T2w (a) and axial T1w (b) images show left inguinal hernia containing fat and a small bowel loop (black arrows). Axial T2w image (c) shows a left fluid-filled distended iliopsoas bursa (white arrowhead), in keeping with iliopsoas bursitis. At the level of the left great adductor, a large regular and homogeneous formation (white asterisks), appearing hyperintense on both T2w (d) and T1w (e) images without signs of contrast-enhancement on post-contrast fat-sat T1w (f) image, is shown, suggestive of intramuscular lipoma. T2*w* T2-weighted, *T1w* T1-weighted.

physiologically dilated but clearly visible at MRI. The main causes of its distension are represented by trauma, osteoarthritis, avascular necrosis, rheumatoid arthritis, synovial chondromatosis, gout and pyogenic infection. Iliopsoas bursitis can simulate a mass, or manifest with non-specific hip pain [77]. US can visualize bursa distension and inform about the contents and presence of septa. However, MRI is generally superior to other imaging modalities in showing a communication between the bursa and the hip and to accurately quantify the degree of distension (Fig. 14c) [78].

2.3.1.3. Intramuscular lipoma. Lipomas are common soft tissue tumors, typically arising subcutaneously and consisting of mature fatty tissue; however, they can less frequently occur under the enclosing fascia (deep-seated lipomas) or even inside the muscle (intramuscular lipomas) [79]. These usually asymptomatic masses appear isointense to subcutaneous fat in all MRI sequences and can greatly differ in terms of dimensions (Fig. 14d–f) [80]. They can present with smooth and regular margins or with infiltrative patterns with the presence of intermingled muscle fibers within the lipoma, which do not represent signs of malignancy. However, the differential diagnosis with well-differentiated liposarcoma or atypical lipomatous tumors is often challenging. The MRI signs suggestive for liposarcoma include tumor heterogeneity, the presence of septa showing enhancement on DCE and/or of non-adipose nodular soft-tissue components; incomplete fat suppression with hyperintense components on T2w images could also raise suspicion [81].

2.3.1.4. Butterfly vertebrae. A butterfly vertebra is a sagittal defect in the vertebral body caused by failure of fusion of the two lateral ossification centers due to persistence of the notochord during embryogenesis (Fig. 15a–b) [82]. The name is based on the appearance of the two hemivertebrae that spread out like butterfly wings from the central cleft on plain radiograph images. In a previous systematic review [83], this pathology seems to be associated in 70 % of cases with other vertebral anomalies and in 56 % of cases as part of more complex syndromes, the most common being spondylocostal dysostosis followed by Alagille syndrome. Vertebral involvement can be single (61 %) or multiple (39 %) with a strong association between multiple involvement and the presence of complex syndromes. The most frequent location is the thoracolumbar region, being especially infrequent at the sacral level. Most cases are asymptomatic, with back pain as the most frequent clinical manifestation.

2.3.1.5. Paget disease. Paget's disease of bone is a common disorder that can involve one or more skeletal segments (more frequently the pelvis), characterized by focal areas of increased bone turnover [84]. Rarely encountered in young adults, its prevalence increases with age, being higher in elder males. Mostly asymptomatic, it is often incidentally discovered on imaging exams performed for other reasons, although bone pain can be present. While Paget's disease shows distinctive radiographic features that allow to confidently make a diagnosis, MRI may present a confusing picture. Uncomplicated Paget's disease can present with cortical thickening (hypointense on both T1w and T2w images) and bone marrow signal abnormalities (Fig. 15c-d) [85]. The most common complication of Paget's disease is represented by fractures, but arthropathy and neurologic complications have been also widely reported. Of note, MRI can have a role in the diagnosis of sarcomatous transformation, which is very rare but constitutes the most

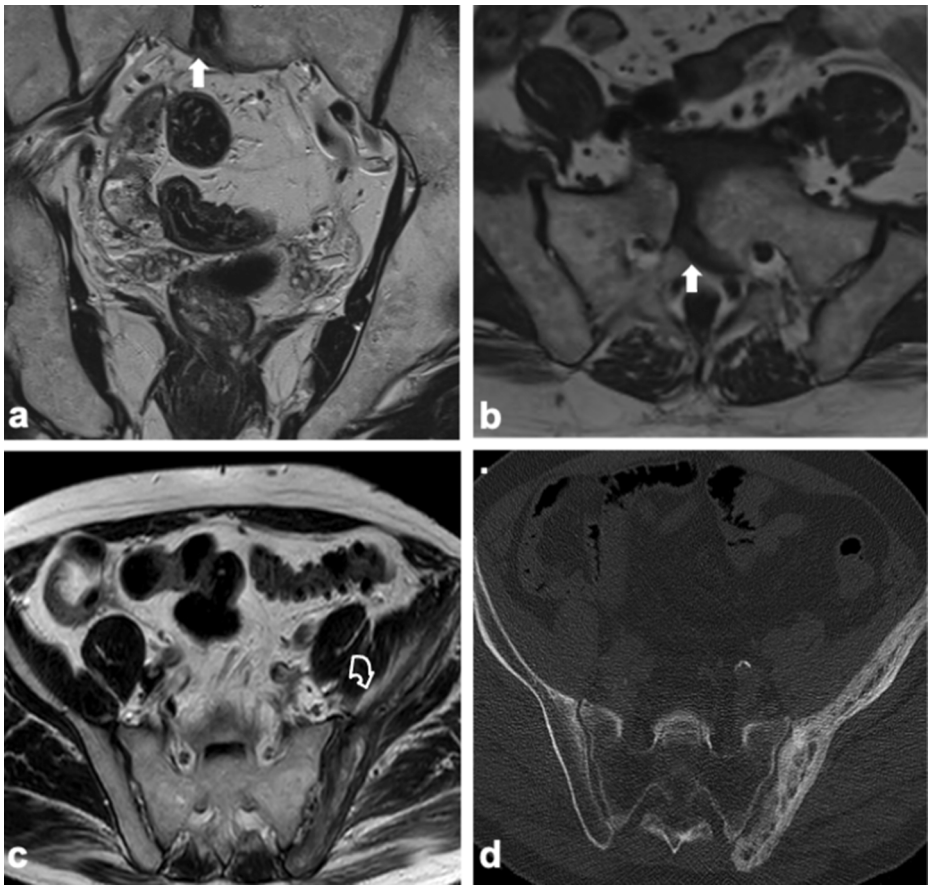

Fig. 15. Coronal (a) and axial (b) T2w images show a cleft in the vertebral body of S1 (arrows), in keeping with Butterfly vertebra. Axial T2w image (c) scan shows thickened cortex, coarse trabeculation and bone sclerosis of the left iliac bone (curved arrow), then confirmed on axial CT image (d), suggestive of Paget disease. *T2w* T2-weighted, *CT* computed tomography.

dreaded complication [86].

2.3.1.6. Osteoarthritis. It is well-known that osteoarthritis represents a significant source of pain and functional limitation [87]. Given it affects adult patients, with a prevalence which increases with age, it should not be considered an uncommon finding in patients referred to MRI for PCa suspicion. The hip represents most involved site in pelvic osteoarthritis and is frequently included in the FOV of prostate MRI. While radiography represents the main imaging modality, MRI offers a greater amount of information on the state of articular cartilage and subchondral bone (Fig. 16). It has been shown that the presence of cartilage alterations, such as fissuring or ulcerations in the weight-bearing areas, especially if paired with bone marrow edema-like changes in the subchondral bone, are correlated to the presence of pain in coxofemoral osteoarthritis [88]. As these MRI signs typically precede radiographic evidence of osteoarthritis, it may be useful to report them as incidental findings when present [89].

2.3.1.7. Femoral geodes. A geode is a hollow rock lined with crystals. The term cyst is inaccurate because subchondral cysts lack an epithelial lining and are not uniformly fluid filled [90]. They are commonly associated with osteoarthritis and are usually multiple, located on opposing sides of the weight-bearing joints. Geodes themselves are generally asymptomatic, however due to concomitant joint pathology they may be associated with non-specific symptoms such as pain, swelling or reduced range of motion. At MRI, they appear as well-defined periarticular lesions, hypointense on T1w, hyperintense on T2w, with heterogenous behavior after gadolinium administration, ranging from absent to peripheral or internal enhancement due to fibrous content (Fig. 16) [91]. Common accompanying diagnostic clues for MRI diagnosis include the formation of osteophytes, the absence of overlying cartilage, joint space narrowing, and the presence of marked surrounding bone oedema. Main differential diagnoses include lytic malignancies, chondroblastoma, giant cell tumor, clear cell chondrosarcoma, or metastases.

2.3.2. Clinically significant

2.3.2.1. Sacrococcygeal chordoma. Chordomas are malignant tumors originating from vestigial notochord tissue, of low to intermediate grade, and are the most common sacral primary bone tumor [92]. Epidemiologically, they interest adult patients with a higher prevalence in males. When arising in the sacrum, they tend to originate in the lower levels of the bone, posteriorly to the rectum. Chordomas present a slow growth, with symptoms mostly related to the spread towards adjacent tissues, especially the presacral space and rectum. Neurological alterations, such as paresthesia, may occur in advanced stages.

Their MRI signal is hypo- to isointense on T1w and markedly hyperintense on T2w images, but may present inhomogeneities due to calcifications, hemorrhage, or high protein content areas; contrast enhancement is present and heterogeneous (Fig. 17a–d) [93]. Differentials include giant cell tumors, which arise in upper levels of the sacrum compared to chordoma and is mostly lytic, and chondrosarcoma, which contains chondroid matrix [94].

2.3.2.2. Bone metastases. Bone secondary lesions are due to hematogenous spread of the primary tumor and can present with varying imaging characteristics based on their origin. They range from osteolytic to osteoblastic, with possible mixed appearance and coexistence of multiple types of bone metastases. On MRI, osteolytic ones may present hypointense appearance on T1w images and iso- to hyperintensity on T2w ones, with heterogeneous enhancement after contrast administration. Osteoblastic metastases characteristically present low signal in both T1w and T2w sequences (Fig. 17e–f) [94]. Their presence can also be associated to other findings, such as pathological fractures due to bone infiltration, even if these are more common in osteolytic lesions. Sacral and pelvic secondary bone tumors can originate from several primary lesions, including prostate, lung, breast, renal, and gastrointestinal cancer. This localization of bone metastases is not infrequent, second only to the other spine segments [95]. As PCa metastases are mostly osteoblastic, this should help in identifying the metastatic lesions as a truly incidental finding in the setting of prostate MRI rather than related to PCa [96].

2.4. Neuro-vascular system

2.4.1. Not clinically significant

2.4.1.1. Tarlov cyst. Tarlov cysts are also known as perineural root sleeve cysts, representing an enlargement of meningeal spaces of the spinal posterior nerve root sheath. Even though their location may include the entire spine, the sacrum and particularly S2 and S3 nerve roots are the most common sites. Such lesions are typically asymptomatic but contain nerve fibers and can present with neurological alterations [97]. These are not highly specific and may include low back pain, radicular pain, paresthesia, leg weakness, bladder or bowel dysfunction [98]. Compared to degenerative changes of the lumbar spine and disc alterations, which may have a similar clinical presentation, Tarlov cysts more often develop in younger adult patients (30–40 years of age).

At MRI, they appear as thin-walled cystic lesions with a signal intensity equal to cerebrospinal fluid and might determine adjacent bone

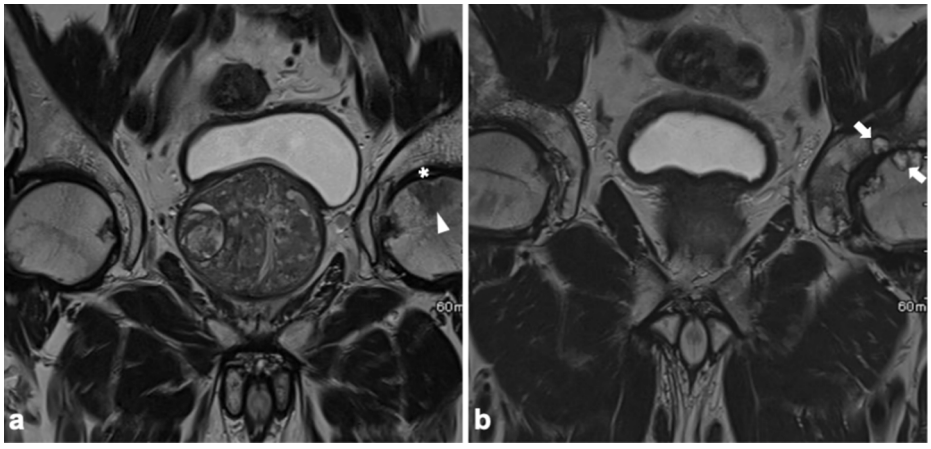

Fig. 16. Coronal T2w images (a–b) show articular cartilage loss (asterisk), bone marrow edema (arrowhead) and subchondral cysts (arrows) at the left femoral head and the acetabular roof in a patient with degenerative osteoarthritis. *T2w* T2-weighted.

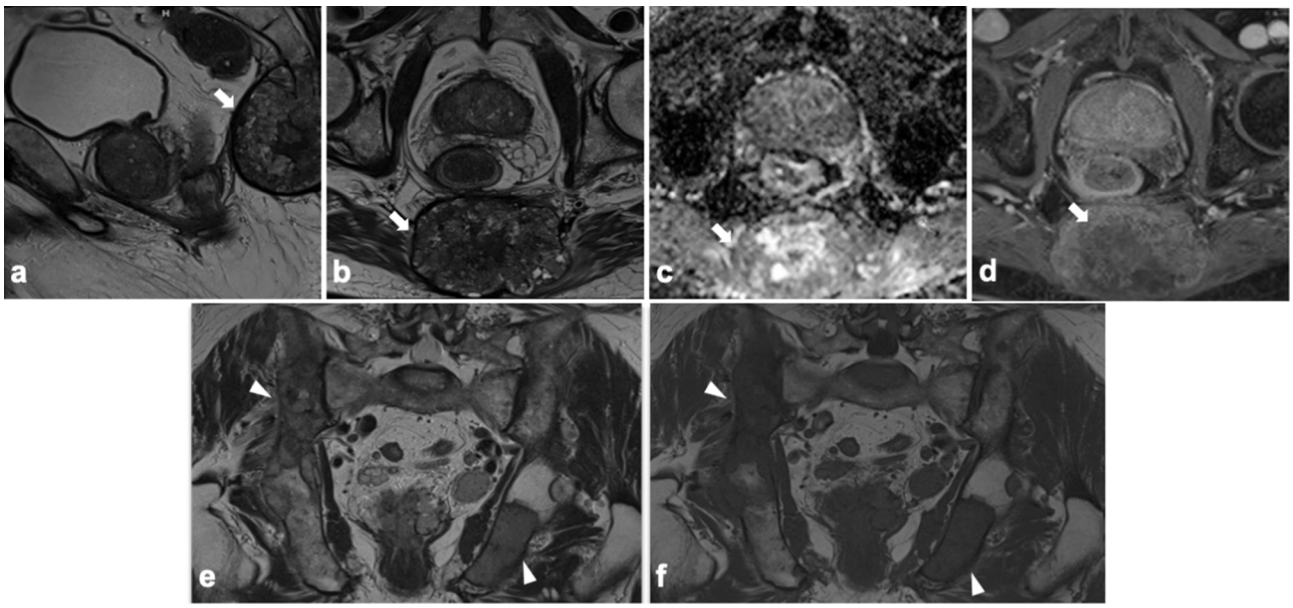

Fig. 17. A large destructive bony mass lesion (arrows) centered upon the coccyx and the fifth sacral vertebra, with inhomogeneous low signal on sagittal (a) and axial (b) T2w images, mostly peripheral restricted diffusion on ADC map (c), heterogeneous enhancement on axial DCE image (d) and extra-osseous extension is shown; the lesion was confirmed at biopsy as sacrococcygeal chordoma. Coronal T2w (e) and T1w (f) images show multiple hypointense lesions localized at pelvic bones (arrowheads), in keeping with metastases. *T2w* T2-weighted, *ADC* apparent diffusion coefficient, *DCE* dynamic contrast enhanced, *T1w* T1-weighted.

scalloping (Fig. 18a). They often present as multiple and or bilateral lesions, without enhancement after contrast agent administration [99].

2.4.1.2. Femoro-femoral bypass. Femoro-femoral bypass is a surgical procedure to sidestep an occluded or injured unilateral iliac artery [100]. A vascular prosthesis is inserted between the femoral arteries through a subcutaneous tunnel. Rarely a subfascial tunnel is created passing in the Retzius space.

Nowadays most patients with symptomatic iliac artery stenosis or occlusion are treated primarily with angioplasty or stenting. Surgery is considered an alternative when endovascular management is not suitable. Direct revascularization is preferred to extra-anatomical bypass because of its superior patency, but for poor-risk patients, femoro-femoral bypass is still a valuable surgical option [101]. Complications of femoro-femoral bypass are graft stenosis or occlusion. On MRI, the prosthesis can have different signal intensities depending on the graft (Fig. 18b–c). A flow void artefact on T2w sequences and arterial enhancement after gadolinium injection is seen if the graft is patent. On T1w sequences, mural thrombus or intimal hyperplasia could be noted as heterogeneous signal intensity.

On prostate MRI is essential to report the presence of a femoro-femoral bypass graft because it can affect the surgical approach in case of prostatectomy.

2.4.2. Clinically significant

2.4.2.1. Periprostatic schwannoma. Schwannomas are benign tumor of the peripheral nerves, usually solitary with slow growth [102].

They represent 5 % of all benign soft tissue tumors mostly located in the head-neck and surfaces of the flexors of the upper and lower limbs, while when deep-seated, they predominate in the posterior mediastinum and retroperitoneum. Schwannomas are often found as an incidental mass or due to vague and non-specific symptoms. Microscopically schwannomas are divided into two categories: highly cellular component or "Antoni A'' and a myxoid or "Antoni B'' component. On MRI schwannomas usually present as well-circumscribed masses displacing but not infiltrating the adjacent structures, hypointense on T1w and hyperintense on T2w images, with heterogenous enhancement after gadolinium administration, being intense in case of "Antoni A" subtype (Fig. 19a–b). Cystic, hemorrhage and fatty degeneration may be present,

Fig. 18. Sagittal T2w image (a) shows a sacral perineural cysts causing minimal bone scalloping of the adiacent vertebra (arrow), also named as Tarlov cyst. Patent femoro-femoral by-pass graft (arrowsheads) characterized by flow void artifact on T2w image (b) and arterial enhancement on axial DCE image (c). A right PI-RADS 5 prostate lesion is also shown in the right posterior mid-gland peripheral zone (curved arrows in b-c). *T2w* T2-weighted, *DCE* Dynamic contrast enhanced.

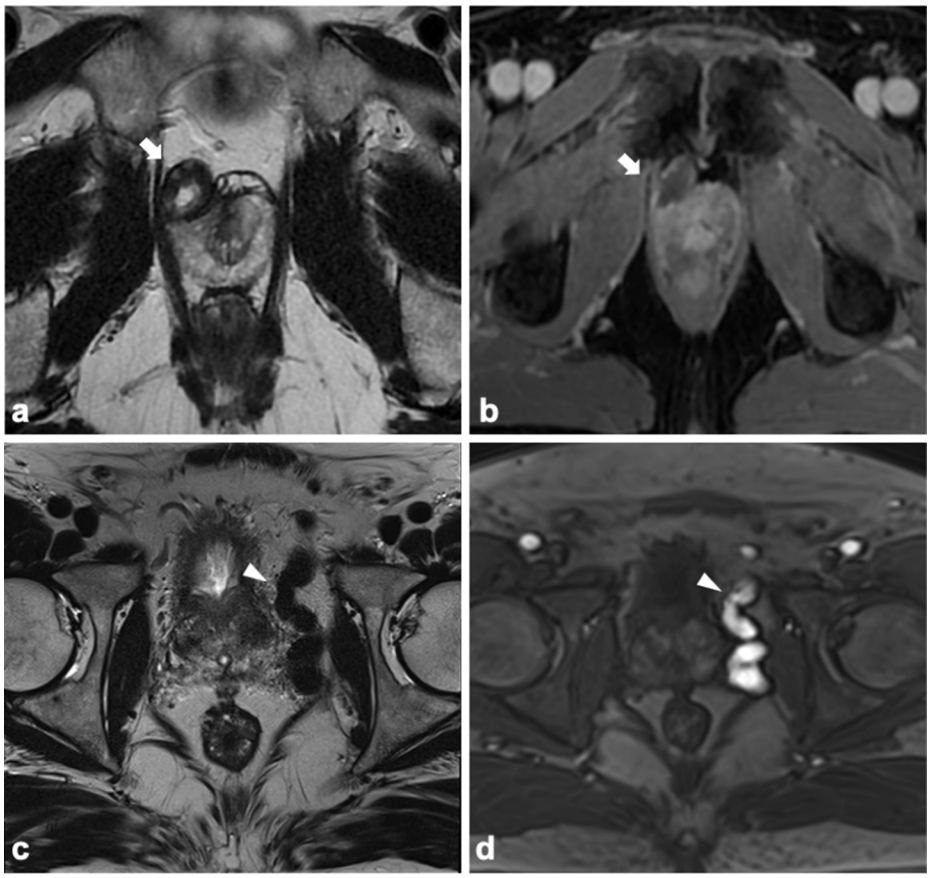

Fig. 19. Axial T2w (a) and post-contrast fat-sat T1w (b) images show a well circumscribed heterogeneous T2-signal mass with peripheral enhancement (arrows) in the right periprostatic space, confirmed at biopsy as schwannoma. Axial T2w image shows ipointense tubular structures in the left *peri*-prostatic space (arrowshead in c), corresponding to ectasic vessels, characterized by precocius arterial enhancement on axial DCE image (arrowshead in d), in keeping with arteriovenous malformation. *T2w* T2-weighted, *T1w* T1-weighted, *DCE* Dynamic contrast enhanced.

while calcifications are rare [103]. Diagnosis of schwannoma may be considered when approaching a retroperitoneal or pelvic mass, to avoid unnecessary surgery, as this disease can be managed conservatively.

2.4.2.2. Pelvic arteriovenous malformation. Arteriovenous malformations consist of abnormal leash of vessels allowing for arteriovenous shunting. They are characterized by a direct arteriovenous communication without intervening capillary bed, being either congenital or acquired. Arteriovenous malformations may occur everywhere, however, the pelvic ones are very rare [104]. Patients may be asymptomatic or present with pelvic pain, painless gross hematuria, hematospermia, urinary frequency. MRI is effective for identifying vascular anomalies, being able to delineate the extent and anatomic relationship of the malformation to adjacent structures as well as to provide hemodynamic characterization (Fig. 19c–d) [105].

Therapeutic options include conservative management, ligation of the inflow artery with excision of the focus, transcatheter arterial embolization and intra-operative embolization of the venous compartment [106].

2.5. Lymphatic system

2.5.1. Not clinically significant

2.5.1.1. Pelvic lymphocele. Lymphocele is a lymph collection with a thick fibrotic wall without an epithelial lining, caused by an injury to the lymphatic system, usually after extraperitoneal surgical procedures [107]. It rarely happens after intraperitoneal surgery because the peritoneum absorbs lymph and prevents lymphocele formation. Lymphocele-related symptoms depend on its location and size due to compression of adjacent anatomic structures or complications like infection. On MRI, lymphoceles appear as simple unilocular cystic masses, usually located along the route of prior lymph node dissection or adjacent to a transplanted kidney [108]. They are highly hyperintense on T2w images, hypointense on T1w, with possible thin wall enhancement on postcontrast T1w images (Fig. 20a–b). Small lymphoceles are generally conservatively managed, with the most regressing over time. Symptomatic lymphoceles treatments include percutaneous drainage with or without sclerotherapy and surgical drainage [109].

2.5.2. Clinically significant

2.5.2.1. Lymphadenopathy. The term lymphadenopathy refers to any pathology of the lymph nodes not only related to the increase in size, which may be normal, but also to structural changes (round, necrotic, cystic). The increase in size indeed is not exclusive of the neoplastic diseases but may also occur due to benign conditions, such as the inflammatory ones [110]. Lymphadenopathy maybe incidentally identified while reporting prostate mpMRI, and in the absence of PCa, this warrants a search for the primary tumor with scrutiny of the bladder and rectum as well as consideration of systemic diseases. If US can be adopted for the evaluation of superficial lymph nodes, CT, PET and MRI are the most used techniques for staging purposes. Both CT and MRI mostly rely on shape and size, considering a short axis diameter greater than 10 mm as suspicious for node metastasis. However, a size-based approach may overlook metastasis, thus MRI accuracy would benefit from the assessment of morphological features such as a more rounded shape or eccentric cortical hypertrophy (Fig. 20c–d).

In a previous metanalysis, Hovels et al. reported that the pooled sensitivity and specificity of MRI to identify metastatic nodes in PCa patients were 39 and 82 %, respectively, being not statistically different from those of CT and MRI [111]. MRI suspicious features of metastatic nodes, beyond increasing in size, include restricted diffusion, central necrosis (visualized as T2w hyperintensity within the node) and lymph

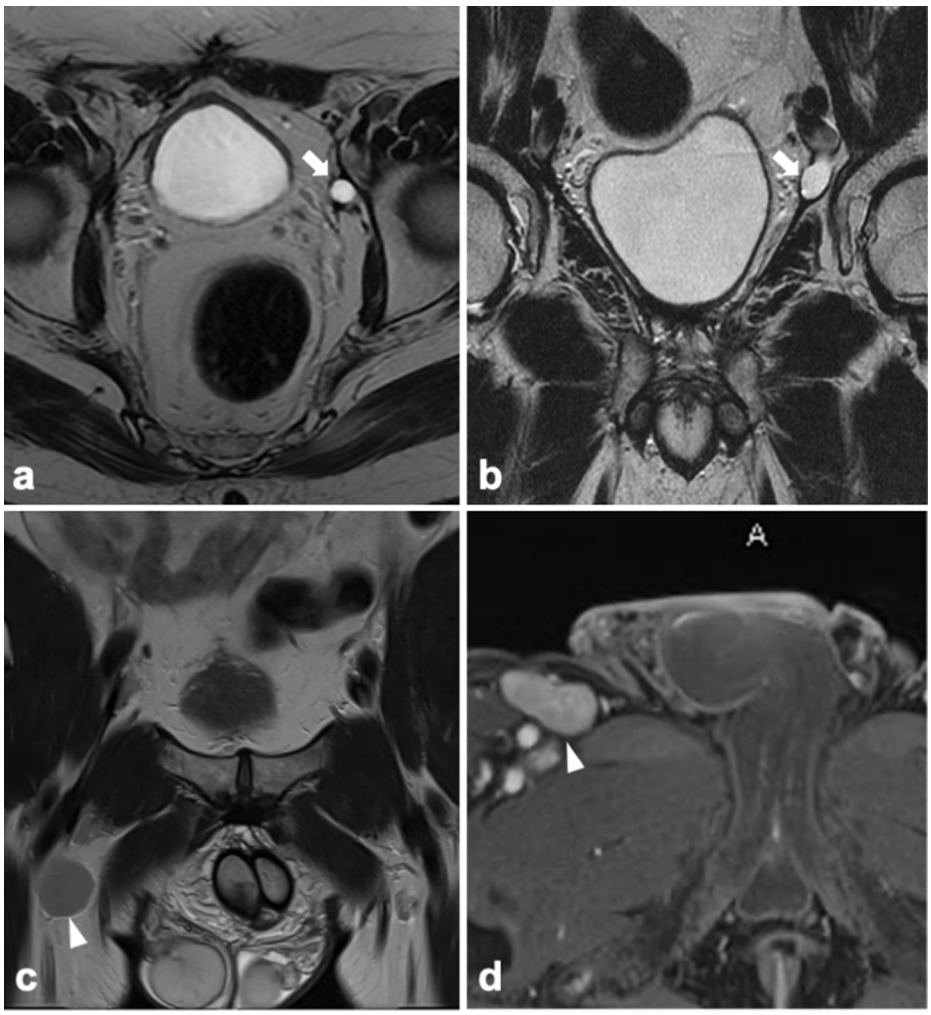

Fig. 20. Axial (a) and coronal (b) T2w images show a small left external iliac capsulated fluid collection (arrows), consistent with lymphocele in a patient underwent radical prostatectomy. Coronal T2w (c) and axial post-contrast fat-sat T1w (d) images show an enlarged right inguinal lymph node (arrowheads), biopsy proven as lymphoma. *T2w* T2-weighted, *T1w* T1-weighted.

node conglomeration [112].

3. Conclusion

Various extra-prostatic findings can be incidentally recognized while reporting mpMRI scans, with a number being clinically significant. Consequently, it is mandatory for a radiologist to be familiar with the anatomical structures included within mpMRI FOV as well as with the wide range of pathologies potentially encountered and their imaging characteristics. A systematic approach consisting in reviewing target areas of each anatomical system by means of a checklist, such as the CheckDEEP, before or after the assessment of the prostate gland, may help in not overlooking those findings which might impact patients' prognosis. Finally, collaboration with referring physicians is needed to guide management and avoid patient anxiety and increased costs due to additional work-up prompted by extra-prostatic findings.

Ethical approval and consent to participate

Not applicable.

Consent for publication:

Images are entirely unidentifiable with no reporting of individual details.

Funding

None.

CRediT authorship contribution statement

Andrea Ponsiglione: Writing – review & editing, Writing – original draft, Methodology, Investigation, Data curation, Conceptualization. **Irene Campo:** Writing – original draft, Writing – review & editing, Conceptualization. **Camilla Sachs:** Writing – original draft, Conceptualization. **Carmelo Sofia:** Writing – original draft, Data curation. **Eduardo Álvarez-Hornia Pérez:** . **Riccardo Ciabattoni:** Writing – original draft, Investigation, Data curation. **Doaa E. Sharaf:** . **Pamela Causa-Andrieu:** Writing – original draft, Visualization, Investigation, Data curation. **Arnaldo Stanzione:** Writing – original draft, Investigation, Data curation. **Renato Cuocolo:** Writing – original draft, Methodology, Data curation. **Jeries Zawaideh:** Writing – original draft, Supervision, Investigation, Data curation. **Giorgio Brembilla:** Supervision, Investigation, Data curation, Conceptualization.

Declaration of Competing Interest

The authors declare the following financial interests/personal relationships which may be considered as potential competing interests: [Dr. Arnaldo Stanzione and Prof. Renato Cuocolo are members of the

European Journal of Radiology Editorial Board but had no involvement in the peer-review of this article and have no access to information regarding its peer-review. The remaining authors declare no conflict of interest.].

Data availability

The data are available from the corresponding author on reasonable request.

Acknowledgements

The authors would like to acknowledge the European Society of Urogenital Radiology. Finally, the Authors would like to thank Professor Alfredo Blandino from University Hospital of Messina for contributing with some of the presented cases.

References

[1] K.W. Doo, D.J. Sung, B.J. Park, M.J. Kim, S.B. Cho, Y.W. Oh, Y.H. Ko, K.S. Yang, Detectability of low and intermediate or high risk prostate cancer with combined T2-weighted and diffusion-weighted MRI, Eur. Radiol. 22 (2012) 1812–1819, https://doi.org/10.1007/s00330-012-2430-5.

[2] R. Cuocolo, F. Verde, A. Ponsiglione, V. Romeo, M. Petretta, M. Imbriaco, A. Stanzione, Clinically significant prostate cancer detection with biparametric MRI: A systematic review and meta-analysis, Am. J. Roentgenol. 216 (2021) 608–621, https://doi.org/10.2214/AJR.20.23219.

[3] J.J. Fütterer, A. Briganti, P. De Visschere, M. Emberton, G. Giannarini, A. Kirkham, S.S. Taneja, H. Thoeny, G. Villeirs, A. Villers, Can clinically significant prostate cancer be detected with multiparametric magnetic resonance imaging? A systematic review of the literature, Eur. Urol. 68 (2015) 1045–1053, https://doi.org/10.1016/j.eururo.2015.01.013.

[4] R. Cuocolo, A. Stanzione, A. Ponsiglione, F. Verde, A. Ventimiglia, V. Romeo, M. Petretta, M. Imbriaco, Prostate MRI technical parameters standardization: A systematic review on adherence to PI-RADSv2 acquisition protocol, Eur. J. Radiol. 120 (2019), 108662, https://doi.org/10.1016/j.ejrad.2019.108662.

[5] EAU Guidelines. Edn. Presented at the EAU Annual Congress Amsterdam 2022. ISBN 978-94-92671-16-5. (n.d.).

[6] B. Turkbey, A.B. Rosenkrantz, M.A. Haider, A.R. Padhani, G. Villeirs, K. J. Macura, C.M. Tempany, P.L. Choyke, F. Cornud, D.J. Margolis, H.C. Thoeny, S. Verma, J. Barentsz, J.C. Weinreb, Prostate imaging reporting and data system version 2.1: 2019 Update of prostate imaging reporting and data system version 2, Eur. Urol. 76 (2019) 340–351, https://doi.org/10.1016/j.eururo.2019.02.033.

[7] J. Trivedi, T. Sutherland, M. Page, Incidental findings in and around the prostate on prostate MRI: a pictorial review, Insights Imag. 12 (2021) 37, https://doi.org/10.1186/s13244-021-00979-7.

[8] C. Christophe, S. Montagne, S. Bourrelier, M. Roupret, E. Barret, F. Rozet, E. Comperat, J.F. Coté, O. Lucidarme, O. Cussenot, B. Granger, R. Renard-Penna, Prostate cancer local staging using biparametric MRI: assessment and comparison with multiparametric MRI, Eur. J. Radiol. 132 (2020), 109350, https://doi.org/10.1016/j.ejrad.2020.109350.

[9] M. de Rooij, E.H.J. Hamoen, J.A. Witjes, J.O. Barentsz, M.M. Rovers, Accuracy of magnetic resonance imaging for local staging of prostate cancer: A diagnostic meta-analysis, Eur. Urol. 70 (2016) 233–245, https://doi.org/10.1016/j.eururo.2015.07.029.

[10] A. Ponsiglione, A. Stanzione, M. Imbriaco, Letter to the Editor regarding "Prostate cancer local staging using biparametric MRI: Assessment and comparison with multiparametric MRI, Eur. J. Radiol. 139 (2021), 109721, https://doi.org/10.1016/j.ejrad.2021.109721.

[11] A. Stanzione, A. Ponsiglione, R. Cuocolo, S. Cocozza, S.G. Picchi, S. Stilo, F. Persico, M. Creta, N. Longo, M. Imbriaco, Abbreviated protocols versus multiparametric MRI for Assessment of extraprostatic extension in prostatic carcinoma: A multireader study, Anticancer Res. 39 (2019) 4449–4454, https://doi.org/10.21873/anticanres.13617.

[12] R.L. Sherrer, W.S. Lai, J.V. Thomas, J.W. Nix, S. Rais-Bahrami, Incidental findings on multiparametric MRI performed for evaluation of prostate cancer, Abdom. Radiol. 43 (2018) 696–701, https://doi.org/10.1007/s00261-017-1237-x.

[13] M.J. Magnetta, R. Catania, R. Girometti, A.C. Westphalen, A.A. Borhani, A. Furlan, Prostate MRI: Staging and decision-making, Abdom. Radiol. 45 (2020) 2143–2153, https://doi.org/10.1007/s00261-020-02431-8.

[14] R.T. Gupta, B. Spilseth, A.T. Froemming, How and why a generation of radiologists must be trained to accurately interpret prostate mpMRI, Abdom. Radiol. 41 (2016) 803–804, https://doi.org/10.1007/s00261-016-0745-4.

[15] G. Cutaia, G. Tosto, R. Cannella, A. Bruno, C. Leto, L. Salvaggio, S. Cutaia, F. P. Lombardo, N. Dispensa, D. Giambelluca, M. Midiri, G. Salvaggio, Prevalence and clinical significance of incidental findings on multiparametric prostate MRI, Radiol. Med. 125 (2020) 204–213, https://doi.org/10.1007/s11547-019-01106-9.

[16] H.-F. Wu, D. Qiao, L.-X. Qian, N.-H. Song, N.-H. Feng, L.-X. Hua, W. Zhang, Congenital agenesis of seminal vesicle, Asian J. Androl. 7 (2005) 449–452, https://doi.org/10.1111/j.1745-7262.2005.00058.x.

[17] C.E. Méndez-Probst, S.E. Pautler, Fusion of the seminal vesicles discovered at the time of robot-assisted laparoscopic radical prostatectomy, J. Robot Surg. 4 (2010) 45–47, https://doi.org/10.1007/s11701-010-0172-4.

[18] O. Ocal, A.D. Karaosmanoglu, M. Karcaaltıncaba, D. Akata, M. Ozmen, Imaging findings of congenital anomalies of seminal vesicles, Pol. J. Radiol. 84 (2019) 25–31, https://doi.org/10.5114/pjr.2019.82711.

[19] S. Zaidi, J. Gandhi, O. Seyam, G. Joshi, W.C. Waltzer, N.L. Smith, S.A. Khan, Etiology, diagnosis, and management of seminal vesicle stones, Curr. Urol. 12 (2019) 113–120, https://doi.org/10.1159/000489429.

[20] M.N. Reddy, S. Verma, Lesions of the seminal vesicles and their MRI characteristics, J. Clin. Imag. Sci. 4 (2014) 61, https://doi.org/10.4103/2156-7514.143734.

[21] E. Maeda, M. Katsura, W. Gonoi, T. Yoshikawa, N. Hayashi, H. Ohtsu, K. Ohtomo, Abnormal signal intensities of the seminal vesicles in a screening population, J. Magnet. Resonan. Imag. 39 (2014) 1426–1430, https://doi.org/10.1002/jmri.24295.

[22] S. Furuya, R. Furuya, N. Masumori, T. Tsukamoto, M. Nagaoka, Magnetic resonance imaging is accurate to detect bleeding in the seminal vesicles in patients with hemospermia, Urology 72 (2008) 838–842, https://doi.org/10.1016/j.urology.2008.05.058.

[23] D.A. Torigian, P. Ramchandani, Hematospermia: imaging findings, Abdom Imag. 32 (2007) 29–49, https://doi.org/10.1007/s00261-006-9013-3.

[24] H.M. Shebel, H.M. Farg, O. Kolokythas, T. El-Diasty, Cysts of the lower male genitourinary tract: Embryologic and anatomic considerations and differential diagnosis, RadioGraphics 33 (2013) 1125–1143, https://doi.org/10.1148/rg.334125129.

[25] A. Hofmann, F. Vauth, W.H. Roesch, Zinner syndrome and infertility—a literature review based on a clinical case, Int. J. Impot. Res. 33 (2021) 191–195, https://doi.org/10.1038/s41443-020-00360-0.

[26] H. Takahashi, T.A. Potretzke, A. Kawashima, J.C. Cheville, S. Masuoka, B. Kim, Imaging of the bulbourethral (cowper) gland: Abnormalities and differential diagnosis, RadioGraphics 42 (2022) 2037–2053, https://doi.org/10.1148/rg.220099.

[27] S. Bugeja, A. Frost, S. Ivaz, M. Dragova, D. Andrich, A. Mundy, Syringoceles of Cowper's ducts and glands in adult men, Asian J. Androl. 22 (2020) 129, https://doi.org/10.4103/aja.aja_59_19.

[28] S. Ramanathan, M. Bertolotto, A. Shamsodini, M. Al Heidous, V. Dogra, P. Ramchandani, Introduction to imaging of penile prostheses: A primer for the radiologist, Am. J. Roentgenol. 210 (2018) 1192–1199, https://doi.org/10.2214/AJR.17.18942.

[29] A.-R. Abualruz, R. O'Malley, J. Ponnatapura, B.L. Holbert, P. Whitworth, R. Tappouni, N. Lalwani, MRI of common penile pathologies and penile prostheses, Abdom. Radiol. 45 (2020) 2825–2839, https://doi.org/10.1007/s00261-019-02080-6.

[30] Y.-T. Chang, J.-Y. Lee, J.-Y. Wang, C.-S. Chiou, C.-C. Chang, Hydrocele of the spermatic cord in infants and children: Its particular characteristics, Urology 76 (2010) 82–86, https://doi.org/10.1016/j.urology.2010.02.062.

[31] M.V. Revzin, D. Ersahin, G.M. Israel, J.D. Kirsch, M. Mathur, J. Bokhari, L. M. Scoutt, US of the inguinal canal: Comprehensive review of pathologic processes with CT and MR imaging correlation, RadioGraphics 36 (2016) 2028–2048, https://doi.org/10.1148/rg.2016150181.

[32] P.J. Woodward, C.M. Schwab, I.A. Sesterhenn, From the archives of the AFIP, RadioGraphics. 23 (2003) 215–240, https://doi.org/10.1148/rg.231025133.

[33] R.A. Kubik-Huch, S. Hailemariam, B. Hamm, CT and MRI of the male genital tract: radiologic-pathologic correlation, Eur Radiol. 9 (1999) 16–28, https://doi.org/10.1007/s003300050621.

[34] W. Kim, M.A. Rosen, J.E. Langer, M.P. Banner, E.S. Siegelman, P. Ramchandani, US–MR imaging correlation in pathologic conditions of the scrotum, RadioGraphics 27 (2007) 1239–1253, https://doi.org/10.1148/rg.275065172.

[35] V.S. Dogra, R.H. Gottlieb, D.J. Rubens, L. Liao, Benign intratesticular cystic lesions: US features, RadioGraphics. 21 (2001) S273–S281, https://doi.org/10.1148/radiographics.21.suppl_1.g01oc15s273.

[36] H. Artas, I. Orhan, Scrotal Calculi, J. Ultrasound Med. 26 (2007) 1775–1779, https://doi.org/10.7863/jum.2007.26.12.1775.

[37] W.T. Malouf, R.B. Dyer, S.C. Carter, Classics in abdominal radiology: a "scrotal pearl", Abdom. Radiol. 44 (2019) 3205–3206, https://doi.org/10.1007/s00261-019-02088-y.

[38] S. Yoshida, R. Takazawa, Y. Uchida, Y. Kohno, Y. Waseda, T. Tsujii, The significance of intraoperative renal pelvic urine and stone cultures for patients at a high risk of post-ureteroscopy systemic inflammatory response syndrome, Urolithiasis 47 (2019) 533–540, https://doi.org/10.1007/s00240-019-01112-6.

[39] C. Siegel, Re: What the radiologist needs to know about urolithiasis: Part 1—Pathogenesis, types, assessment, and variant anatomy, J. Urol. 189 (2013) 173–174, https://doi.org/10.1016/j.juro.2012.09.160.

[40] J.F. Donaldson, Y. Ruhayel, A. Skolarikos, S. MacLennan, Y. Yuan, R. Shepherd, K. Thomas, C. Seitz, A. Petrik, C. Türk, A. Neisius, Treatment of bladder stones in adults and children: A systematic review and meta-analysis on behalf of the European association of urology urolithiasis guideline panel, Eur. Urol. 76 (2019) 352–367, https://doi.org/10.1016/j.eururo.2019.06.018.

[41] C.E. Blane, J.M. Zerin, D.A. Bloom, Bladder diverticula in children, Radiology 190 (1994) 695–697, https://doi.org/10.1148/radiology.190.3.8115613.

[42] J.A. Hutch, Saccule formation at the ureterovesical junction in smooth walled bladders, J. Urol. 86 (1961) 390–399, https://doi.org/10.1016/S0022-5347(17)65186-3.

[43] S. Buddha, C.O. Menias, V.S. Katabathina, Imaging of urachal anomalies, Abdom. Radiol. 44 (2019) 3978–3989, https://doi.org/10.1007/s00261-019-02205-x.

[44] C. ParadaVillavicencio, S.Z. Adam, P. Nikolaidis, V. Yaghmai, F.H. Miller, Imaging of the urachus: Anomalies, complications, and mimics, RadioGraphics 36 (2016) 2049–2063, https://doi.org/10.1148/rg.2016160062.

[45] T. Berrocal, P. López-Pereira, A. Arjonilla, J. Gutiérrez, Anomalies of the distal ureter, bladder, and urethra in children: Embryologic, radiologic, and pathologic features, RadioGraphics 22 (2002) 1139–1164, https://doi.org/10.1148/radiographics.22.5.g02se101139.

[46] J.J. Wong-You-Cheong, P.J. Woodward, M.A. Manning, C.J. Davis, Inflammatory and nonneoplastic bladder masses: Radiologic-pathologic correlation, RadioGraphics 26 (2006) 1847–1868, https://doi.org/10.1148/rg.266065126.

[47] M.D. Timberlake, S.T. Corbett, Minimally invasive techniques for management of the ureterocele and ectopic ureter, Urol. Clin. North Am. 42 (2015) 61–76, https://doi.org/10.1016/j.ucl.2014.09.006.

[48] Y.J. Moon, H.-W. Kim, J.B. Kim, H.J. Kim, Y.-S. Chang, Distribution of ureteral stones and factors affecting their location and expulsion in patients with renal colic, Korean J. Urol. 56 (2015) 717, https://doi.org/10.4111/kju.2015.56.10.717.

[49] W. Brisbane, M.R. Bailey, M.D. Sorensen, An overview of kidney stone imaging techniques, Nat. Rev. Urol. 13 (2016) 654–662, https://doi.org/10.1038/nrurol.2016.154.

[50] M. Jaffer, S. Mitra, S. Mandal, M. Das, R. Mahlingam, P. Nayak, Cystadenoma of the seminal vesicle: A case report of rare seminal vesical tumor and review of literature, Urology. 123 (2019) e11–e14, https://doi.org/10.1016/j.urology.2018.10.032.

[51] A.T. Gentile, H.S. Moseley, S.F. Quinn, D. Franzini, T.M. Pitre, Leiomyoma of the seminal vesicle, J. Urol. 151 (1994) 1027–1029, https://doi.org/10.1016/S0022-5347(17)35159-5.

[52] M. Tarjan, I. Ottlecz, T. Tot, Primary adenocarcinoma of the seminal vesicle, Indian J. Urol. 25 (2009) 143, https://doi.org/10.4103/0970-1591.45557.

[53] I. Caglic, V. Panebianco, H.A. Vargas, V. Bura, S. Woo, M. Pecoraro, S. Cipollari, E. Sala, T. Barrett, MRI of bladder cancer: Local and nodal staging, J. Magnet. Resonan. Imag. 52 (2020) 649–667, https://doi.org/10.1002/jmri.27090.

[54] S. Woo, C.H. Suh, S.Y. Kim, J.Y. Cho, S.H. Kim, Diagnostic performance of MRI for prediction of muscle-invasiveness of bladder cancer: A systematic review and meta-analysis, Eur. J. Radiol. 95 (2017) 46–55, https://doi.org/10.1016/j.ejrad.2017.07.021.

[55] V. Panebianco, Y. Narumi, E. Altun, B.H. Bochner, J.A. Efstathiou, S. Hafeez, R. Huddart, S. Kennish, S. Lerner, R. Montironi, V.F. Muglia, G. Salomon, S. Thomas, H.A. Vargas, J.A. Witjes, M. Takeuchi, J. Barentsz, J.W.F. Catto, Multiparametric magnetic resonance imaging for bladder cancer: Development of VI-RADS (vesical imaging-reporting and data system), Eur. Urol. 74 (2018) 294–306, https://doi.org/10.1016/j.eururo.2018.04.029.

[56] A.L. Lai, Y.M. Law, VI-RADS in bladder cancer: Overview, pearls and pitfalls, Eur. J. Radiol. 160 (2023), 110666, https://doi.org/10.1016/j.ejrad.2022.110666.

[57] A.V. Weizman, G.C. Nguyen, Diverticular disease: Epidemiology and management, Canadian J. Gastroenterol. 25 (2011) 385–389, https://doi.org/10.1155/2011/795241.

[58] M.J. Snyder, Imaging of colonic diverticular disease, Clin. Colon. Rectal Surg. 17 (2004) 155–162, https://doi.org/10.1055/s-2004-832696.

[59] O. Buckley, T. Geoghegan, G. McAuley, T. Persaud, F. Khosa, W.C. Torreggiani, Pictorial review: magnetic resonance imaging of colonic diverticulitis, Eur. Radiol. 17 (2007) 221–227, https://doi.org/10.1007/s00330-006-0236-z.

[60] M. Karcaaltincaba, D. Karcaaltincaba, A. Ayhan, Diagnosis of tailgut cysts, Am. J. Roentgenol. 185 (2005) 1369–1370, https://doi.org/10.2214/AJR.05.5148.

[61] K.S. Hain, P.J. Pickhardt, M.G. Lubner, C.O. Menias, S. Bhalla, Presacral masses: Multimodality imaging of a multidisciplinary space, RadioGraphics 33 (2013) 1145–1167, https://doi.org/10.1148/rg.334115171.

[62] V. Lohsiriwat, Hemorrhoids: From basic pathophysiology to clinical management, World J. Gastroenterol. 18 (2012) 2009, https://doi.org/10.3748/wjg.v18.i17.2009.

[63] P. Guniganti, S. Lewis, A. Rosen, S. Connolly, C. Raptis, V. Mellnick, Imaging of acute anorectal conditions with CT and MRI, Abdom. Radiol. 42 (2017) 403–422, https://doi.org/10.1007/s00261-016-0982-6.

[64] I. Gardner, Benign anorectal disease: hemorrhoids, fissures, and fistulas, Ann. Gastroenterol. (2019), https://doi.org/10.20524/aog.2019.0438.

[65] L. Peyrin-Biroulet, J. Panés, W.J. Sandborn, S. Vermeire, S. Danese, B.G. Feagan, J.-F. Colombel, S.B. Hanauer, B. Rycroft, Defining disease severity in inflammatory bowel diseases: Current and future directions, Clin. Gastroenterol. Hepatol. 14 (2016) 348–354.e17, https://doi.org/10.1016/j.cgh.2015.06.001.

[66] G. Masselli, G. Gualdi, MR Imaging of the Small Bowel, Radiology. 264 (2012) 333–348, https://doi.org/10.1148/radiol.12111658.

[67] G. Argilés, J. Tabernero, R. Labianca, D. Hochhauser, R. Salazar, T. Iveson, P. Laurent-Puig, P. Quirke, T. Yoshino, J. Taieb, E. Martinelli, D. Arnold, Localised colon cancer: ESMO clinical practice guidelines for diagnosis, treatment and follow-up, Ann. Oncol. 31 (2020) 1291–1305, https://doi.org/10.1016/j.annonc.2020.06.022.

[68] T. Sawicki, M. Ruszkowska, A. Danielewicz, E. Niedźwiedzka, T. Arłukowicz, K. E. Przybyłowicz, A review of colorectal cancer in terms of epidemiology, risk factors, development, symptoms and diagnosis, Cancers (Basel). 13 (2021) 2025, https://doi.org/10.3390/cancers13092025.

[69] N. Horvat, C. CarlosTavaresRocha, B. Clemente Oliveira, I. Petkovska, M. J. Gollub, MRI of rectal Cancer: Tumor staging, imaging techniques, and management, RadioGraphics 39 (2019) 367–387, https://doi.org/10.1148/rg.2019180114.

[70] J.A. Rizzo, A.L. Naig, E.K. Johnson, Anorectal abscess and fistula-in-ano: Evidence-based management, Surg. Clin. North Am. 90 (2010) 45–68, https://doi.org/10.1016/j.suc.2009.10.001.

[71] J. de Miguel Criado, L.G. del Salto, P.F. Rivas, L.F.A. del Hoyo, L.G. Velasco, M.I. D.P. de las Vacas, A.G. Marco Sanz, M.M. Paradela, E.F. Moreno, MR imaging evaluation of perianal fistulas: Spectrum of imaging features, RadioGraphics 32 (2012) 175–194, https://doi.org/10.1148/rg.321115040.

[72] A. Dohan, C. Eveno, R. Oprea, K. Pautrat, V. Placé, M. Pocard, C. Hoeffel, M. Boudiaf, P. Soyer, Diffusion-weighted MR imaging for the diagnosis of abscess complicating fistula-in-ano: preliminary experience, Eur. Radiol. 24 (2014) 2906–2915, https://doi.org/10.1007/s00330-014-3302-y.

[73] Y.Z. Tang, T.C. Booth, D. Swallow, K. Shahabuddin, M. Thomas, D. Hanbury, S. Chang, C. King, Imaging features of colovesical fistulae on MRI, Br. J. Radiol. 85 (2012) 1371–1375, https://doi.org/10.1259/bjr/55871151.

[74] T. Golabek, A. Szymanska, T. Szopinski, J. Bukowczan, M. Furmanek, J. Powroznik, P. Chlosta, Enterovesical fistulae: Aetiology imaging, and management, Gastroenterol. Res. Pract. 2013 (2013) 1–8, https://doi.org/10.1155/2013/617967.

[75] M.C. Cabarrus, B.M. Yeh, A.S. Phelps, J.J. Ou, S.C. Behr, From Inguinal hernias to spermatic cord lipomas: Pearls, pitfalls, and mimics of abdominal and pelvic hernias, RadioGraphics 37 (2017) 2063–2082, https://doi.org/10.1148/rg.2017170070.

[76] K.P. Murphy, O.J. O'Connor, M.M. Maher, Adult abdominal hernias, Am. J. Roentgenol. 202 (2014) W506–W511, https://doi.org/10.2214/AJR.13.12071.

[77] D.G. Varma, W.R. Richli, C. Charnsangavej, B.I. Samuels, E.E. Kim, S. Wallace, MR appearance of the distended iliopsoas bursa, Am. J. Roentgenol. 156 (1991) 1025–1028, https://doi.org/10.2214/ajr.156.5.2017926.

[78] P. Wunderbaldinger, C. Bremer, E. Schellenberger, M. Cejna, K. Turetschek, F. Kainberger, Imaging features of iliopsoas bursitis, Eur. Radiol. 12 (2002) 409–415, https://doi.org/10.1007/s003300101041.

[79] S. McTighe, I. Chernev, Intramuscular lipoma: a review of the literature, Orthop Rev (Pavia). 6 (2014), https://doi.org/10.4081/or.2014.5618.

[80] P. Gupta, T.A. Potti, S.D. Wuertzer, L. Lenchik, D.A. Pacholke, Spectrum of fat-containing soft-tissue masses at MR imaging: The common, the uncommon, the characteristic, and the sometimes confusing, RadioGraphics 36 (2016) 753–766, https://doi.org/10.1148/rg.2016150133.

[81] A. Elbardouni, M. Kharmaz, M. Salah Berrada, M. Mahfoud, M. Elyaacoubi, Well-circumscribed deep-seated lipomas of the upper extremity. A report of 13 cases, Orthopaed. Traumatol. Surg. Res. 97 (2011) 152–158, https://doi.org/10.1016/j.otsr.2010.09.019.

[82] K.M. Kaplan, J.M. Spivak, J.A. Bendo, Embryology of the spine and associated congenital abnormalities, Spine J. 5 (2005) 564–576, https://doi.org/10.1016/j.spinee.2004.10.044.

[83] Y. Katsuura, H.J. Kim, Butterfly vertebrae: A systematic review of the literature and analysis, Global Spine J. 9 (2019) 666–679, https://doi.org/10.1177/2192568218801016.

[84] S.H. Ralston, Paget's disease of bone, N Eng. J. Med. 368 (2013) 644–650, https://doi.org/10.1056/NEJMcp1204713.

[85] K. Cortis, K. Micallef, A. Mizzi, Imaging Paget's disease of bone—from head to toe, Clin. Radiol. 66 (2011) 662–672, https://doi.org/10.1016/j.crad.2010.12.016.

[86] D.J. Theodorou, S.J. Theodorou, Y. Kakitsubata, Imaging of Paget disease of bone and its musculoskeletal complications: Review, Am. J. Roentgenol. 196 (2011) S64–S75, https://doi.org/10.2214/AJR.10.7222.

[87] F.W. Roemer, S. Demehri, P. Omoumi, T.M. Link, R. Kijowski, S. Saarakkala, M. D. Crema, A. Guermazi, State of the Art: Imaging of Osteoarthritis—Revisited 2020, Radiology 296 (2020) 5–21, https://doi.org/10.1148/radiol.2020192498.

[88] A.J. Teichtahl, Y. Wang, S. Smith, A.E. Wluka, G.G. Giles, K.L. Bennell, R. O'Sullivan, F.M. Cicuttini, Structural changes of hip osteoarthritis using magnetic resonance imaging, Arthritis Res Ther. 16 (2014) 466, https://doi.org/10.1186/s13075-014-0466-4.

[89] H. Kijima, S. Yamada, N. Konishi, H. Kubota, H. Tazawa, T. Tani, N. Suzuki, K. Kamo, Y. Okudera, M. Fujii, K. Sasaki, T. Kawano, Y. Iwamoto, I. Nagahata, T. Miura, N. Miyakoshi, Y. Shimada, The differences in imaging findings between painless and painful osteoarthritis of the hip, Clin. Med. Insights Arthritis Musculoskelet Disord. 13 (2020), https://doi.org/10.1177/1179544120946747, 117954412094674.

[90] L.W. Bancroft, J.J. Peterson, M.J. Kransdorf, Cysts, geodes, and erosions, Radiol. Clin. North Am. 42 (2004) 73–87, https://doi.org/10.1016/S0033-8389(03)00165-9.

[91] E. Perdikakis, V. Skiadas, MRI characteristics of cysts and "cyst-like" lesions in and around the knee: what the radiologist needs to know, Insights, Imaging 4 (2013) 257–272, https://doi.org/10.1007/s13244-013-0240-1.

[92] J. Llauger, J. Palmer, S. Amores, S. Bague, A. Camins, Primary tumors of the sacrum, Am. J. Roentgenol. 174 (2000) 417–424, https://doi.org/10.2214/ajr.174.2.1740417.

[93] K. Farsad, S.V. Kattapuram, R. Sacknoff, J. Ono, G.P. Nielsen, Sacral chordoma, RadioGraphics 29 (2009) 1525–1530, https://doi.org/10.1148/rg.295085215.

[94] E. Vanheule, W. Huysse, N. Herregods, K. Verstraete, L. Jans, Sacral tumours on MRI: A pictorial essay, J. Belg. Soc. Radiol. 103 (2019), https://doi.org/10.5334/jbsr.1887.

[95] Q. Yang, N. Chen, W. Fu, Clinical features and outcomes of metastatic bone tumors of the pelvis, J. Int. Med. Res. 49 (2021), https://doi.org/10.1177/03000605211013152, 030006052110131.
[96] A.A. Ho, S.S. Khara, D.J. Ferguson, M.F. Mohammed, S.D. Chang, A.C. Harris, A PSA for radiologists: Pictorial review of incidentalomas on prostate magnetic resonance imaging, Canadian Assoc. Radiol. J. 70 (2019) 134–146, https://doi.org/10.1016/j.carj.2018.09.005.
[97] C. Lucantoni, K.D. Than, A.C. Wang, J.M. Valdivia-Valdivia, C.O. Maher, F. La Marca, P. Park, Tarlov cysts: a controversial lesion of the sacral spine, Neurosurg. Focus. 31 (2011) E14, https://doi.org/10.3171/2011.9.FOCUS11221.
[98] H. Mieke, B. Frans, S. Alix, S. Ingeborg, P. Benjamin, V. Greet, R. Rasschaert, D. M. Peter, D. Wim, Electromyography and A Review of the literature provide insights into the role of sacral perineural cysts in unexplained chronic pelvic, perineal and leg pain syndromes, Int. J. Phys. Med. Rehabil. 05 (2017), https://doi.org/10.4172/2329-9096.1000407.
[99] M. Shoyab, Tarlov cysts in back pain patients: prevalence, measurement method and reporting points, Br. J. Radiol. 94 (2021), https://doi.org/10.1259/bjr.20210505.
[100] L. Capoccia, V. Riambau, M. da Rocha, Is femorofemoral crossover bypass an option in claudication? Ann. Vasc. Surg. 24 (2010) 828–832, https://doi.org/10.1016/j.avsg.2010.03.021.
[101] H. Lau, S.W.K. Cheng, J. Hui, Eighteen-year experience with femoro-femoral bypass, ANZ J. Surg. 70 (2000) 275–278, https://doi.org/10.1046/j.1440-1622.2000.01806.x.
[102] N.J. Lee, R.H. Hruban, E.K. Fishman, Abdominal schwannomas: review of imaging findings and pathology, Abdom. Radiol. 42 (2017) 1864–1870, https://doi.org/10.1007/s00261-017-1088-5.
[103] M.J. Hughes, J.M. Thomas, C. Fisher, E.C. Moskovic, Imaging features of retroperitoneal and pelvic schwannomas, Clin. Radiol. 60 (2005) 886–893, https://doi.org/10.1016/j.crad.2005.01.016.
[104] K.D. Calligaro, T.V. Sedlacek, R.P. Savarese, P. Carneval, D.A. DeLaurentis, Congenital pelvic arteriovenous malformations: Long-term follow-up in two cases and a review of the literature, J. Vasc. Surg. 16 (1992) 100–108, https://doi.org/10.1016/0741-5214(92)90425-8.
[105] U. Bashir, S. Shah, S. Jeph, M. O'Keeffe, F. Khosa, Magnetic resonance (MR) imaging of vascular malformations, Pol. J. Radiol. 82 (2017) 731–741, https://doi.org/10.12659/PJR.903491.
[106] R. Houbballah, A. Mallios, B. Poussier, P. Soury, S. Fukui, F. Gigou, C. Laurian, A new therapeutic approach to congenital pelvic arteriovenous malformations, Ann. Vasc. Surg. 24 (2010) 1102–1109, https://doi.org/10.1016/j.avsg.2010.02.053.
[107] J.H. Hwang, B.W. Kim, The incidence of postoperative symptomatic lymphocele after pelvic lymphadenectomy between abdominal and laparoscopic approach: a systemic review and meta-analysis, Surg. Endosc. 36 (2022) 7114–7125, https://doi.org/10.1007/s00464-022-09227-5.
[108] T.M. Hegazi, A.M. Al-Sharydah, K.S. Lee, K. Mortele, Retroperitoneal cystic masses: magnetic resonance imaging features, Abdom. Radiol. 45 (2020) 499–511, https://doi.org/10.1007/s00261-019-02246-2.
[109] M. Karcaaltincaba, O. Akhan, Radiologic imaging and percutaneous treatment of pelvic lymphocele, Eur. J. Radiol. 55 (2005) 340–354, https://doi.org/10.1016/j.ejrad.2005.03.007.
[110] P. Zeppa, I. Cozzolino, Lymphadenitis and Lymphadenopathy, 2018, pp. 19–33, doi: 10.1159/000478879.
[111] A.M. Hövels, R.A.M. Heesakkers, E.M. Adang, G.J. Jager, S. Strum, Y. L. Hoogeveen, J.L. Severens, J.O. Barentsz, The diagnostic accuracy of CT and MRI in the staging of pelvic lymph nodes in patients with prostate cancer: a meta-analysis, Clin. Radiol. 63 (2008) 387–395, https://doi.org/10.1016/j.crad.2007.05.022.
[112] Y. Mao, S. Hedgire, M. Harisinghani, Radiologic assessment of lymph nodes in oncologic patients, Curr. Radiol. Rep. 2 (2014) 36, https://doi.org/10.1007/s40134-013-0036-6.